Flanders
State of
the Art

18_135_1
FH Reports

Numerical study of fish passage entrances annex to Denderleeuw's weir-lock complex

Preliminary assessment of flow attraction performance and revision of previous studies

DEPARTMENT
MOBILITY &
PUBLIC
WORKS

www.flandershydraulics.be

Numerical study of fish passage entrances annex to Denderleeuw's weir-lock complex

Preliminary assessment of flow attraction performance and revision of previous studies

López Castaño, S.; Van Hoydonck, W.; Visser, K. P.; Verelst, K.

Flanders Hydraulics
Flanders State of the Art

Legal notice

Copyright and citation

D/2025/3241/132

This publication should be cited as follows:

López Castaño, S.; Van Hoydonck, W.; Visser, K. P.; Verelst, K. (2025). Numerical study of fish passage entrances annex to Dender-leeuw's weir-lock complex: Preliminary assessment of flow attraction performance and revision of previous studies. Version 3.0. FH Reports, 18_135_1. Flanders Hydraulics: Antwerp

Document identification

Customer:	Flanders Hydraulics	Ref.:	WL2025R18_135_1
Keywords (3-5):	CFD, fish passages		
Knowledge domains:	Hydraulic Structures > Fishpasses > Fishpass entrance and attraction > Numerical Modelling		
Text (p.):	31	Appendices (p.):	25
Confidential:	No	☒ Available online	

Author(s):	López Castaño, S.

Control

	Name	Signature
Revisor(s):	Van Hoydonck, W.; Visser, K. P.	Getekend door:Van Hoydonck Wim Rik M Getekend op:2025-04-23 20:37:51 +02:0 Reden:Ik keur dit document goed Van Hoydonck Wim Vlaamse overheid Getekend door:Klaas Visser (Signature) Getekend op:2025-04-24 15:29:25 +02:0 Reden:Ik keur dit document goed Visser Klaas Pieter Vlaamse overheid
Project leader:	Verelst, K.	Getekend door:Kristof Verelst (Signature) Getekend op:2025-04-23 16:30:48 +02:0 Reden:Ik keur dit document goed Verelst Kristof Vlaamse overheid

Approval

Head of division:	Bellafkih, A.	Getekend door:Abdelkarim Bellafkih (Sign Getekend op:2025-04-24 10:12:36 +02:0 Reden:Ik keur dit document goed Bellafkih Abdelkarim Vlaamse overheid

Abstract

The hydrodynamic features of several design alternatives for the entrance of the fish passage annex to the Denderleeuw's lock-weir complex are studied by means of the Volume-of-Fluid (VoF) method using Computational Fluid Dynamics (CFD). These accessories are meant to enhance the fish attraction performance of the fish passage attached to the lock-weir complex in Denderleeuw. Previous studies performed by Badano *et al.* (2019) for the fish passage in Denderleeuw show favorable currents going through the entrance of the fishpass, and overall flow velocities somewhat below the upper threshold defined by the designer. However, studies conducted here show increased flow bulking and aeration downstream of the weir, plus diminished flow attraction due to the sheer difference in specific forces between the flow exiting the fish passage and the flow produced by the weirs. The present results differ from previous studies, and may lead to different assessments. Therefore, the present work attempts to provide further explanation to the aforementioned phenomena and to critically assess the differences between the previous and the present study.

Contents

Abstract III

List of Figures VI

List of Tables VIII

Nomenclature IX

1 Introduction 1
1.1 Objectives 1
1.2 Fish attraction assessment criteria 2
1.3 Contents 2

2 Simulation settings and preliminaries 3
2.1 Governing equations and turbulence model 3
2.2 Boundary conditions and parameters 3
2.2.1 Adaptive Mesh Refinement (AMR) of Polyhedra 3

I Modelling of the attraction flow towards the fish passage's entrance 5

3 Previous CFD studies 6
3.1 Overview 6
3.2 Simulations conducted by IMDC 7
3.2.1 S2-A case 8
3.2.2 S2-B case 8
3.2.3 S2-A: verifications conducted by FH 9

4 Simulations conducted by FH 13
4.1 Baseline case 14
4.2 Alternative with vanes and confluence contraction 14
4.3 Concluding Remarks 14

II Modelling of the added flow in the outflow channel 18

5 CFD studies 19
5.1 General 19
5.2 Simulations conducted by IMDC 19
5.2.1 S1-A: No guide vanes 20
5.2.2 S1-B and S1-C: guide vanes 22
5.3 Simulations conducted by FH 23
5.3.1 Added flow: Submerged slanted intake 24
5.3.2 Added flow: two basins and contraction 25
5.4 Concluding remarks 26

References 30

A1 Flow patterns in aerated flow: theory and numerical analysis A1
A1.1 On the mechanisms producing local losses in the absence of aeration A1
A1.2 On the mechanisms producing local losses in aerated flows A5
A1.3 Concluding Remarks A6
A1.3.1 Future research A7

A2 Post-procesing of simulations conducted by FH A10
A2.1 Modelling of the attraction flow in the tailbay A10
A2.1.1 BASELINE Case A12
A2.1.2 ALTERNATIVE 1 Case A19

List of Figures

Figure 1 Planview of the Denderleeuw lock in Dender. 1
Figure 2 Numerical domain considered for studying the attraction flow at the fishpass's entrance. 7
Figure 3 Iso-contours of mean velocity and air-water phase-fraction for simulation S2-A, conducted by International Maritime and Dredging Consultants (IMDC). The origin of coordinates is chosen arbitrarily for the horizontal axes. 10
Figure 4 Iso-contours of mean velocity and mass phase-fraction for simulation S2-B, conducted by IMDC. 11
Figure 5 Iso-contours of mean velocity and mass phase-fraction for simulation S2-A, conducted by Flanders Hydraulics (FH). 12
Figure 6 Geometry of the main channel and fish passage entrance for the simulations conducted by FH. Note the baseline case includes no vanes, while alternative 1 includes vanes and a side-wall contraction at the left bank. 13
Figure 7 Results obtained for the baseline simulation conducted by FH. 16
Figure 8 Results obtained for the baseline simulation conducted by FH. 17
Figure 9 Fish pass outflow and added flow alternatives proposed by Visser *et al.* (2024). 19
Figure 10 Mesh topology and guide vane configurations proposed in Badano *et al.* (2019). 20
Figure 11 Simulation results for the S1-A case run by Badano *et al.* (2019). 21
Figure 12 Simulation results for the S1-B case run by Badano *et al.* (2019). 22
Figure 13 Simulation results for the S1-C case run by Badano *et al.* (2019). 23
Figure 14 Submerged slanted intake case. 24
Figure 15 Unsteadiness of the flow through the knife gate. 25
Figure 16 Added flow with two basins and a contraction in the fish passage entrance. 27
Figure 17 Results for high added flow with two basins and a contraction in the fish passage entrance. 28
Figure 18 Results for low added flow with two basins and a contraction in the fish passage entrance. 29
Figure 19 Analysis of section of the weir complex for scenario S2-A. A3
Figure 20 Results obtained for the two idealizations studied. No bottom roller is seen in either case. A5
Figure 21 Analysis of section of the weir complex for scenario S2-A-FH. A8
Figure 22 VoF Results obtained for the idealization studied: (a) considering aeration and density variations at section 1, and (b) ignoring aeration. Note the shear region of the roller upstream occurs where the iso-contours of α are the closest for the aerated case. A9
Figure 23 Horizontal and vertical cross sections requested within the frame of the present project. A11
Figure 24 Horizontal plane at Z = 5.5 mTAW. A12
Figure 25 Horizontal plane at Z = 6.0 mTAW. A12
Figure 26 Horizontal plane at Z = 6.5 mTAW. A13
Figure 27 Horizontal plane at Z = 7.0 mTAW. A13
Figure 28 Horizontal plane at Z = 7.5 mTAW. A14
Figure 29 Vertical Plane at Section 1. ..... A14
Figure 30 Vertical Plane at Section 2. ..... A15
Figure 31 Vertical Plane at Section 3. ..... A15
Figure 32 Vertical Plane at Section 4. ..... A16
Figure 33 Vertical Plane at Section 5. ..... A16
Figure 34 Vertical Plane at Section 6. ..... A17
Figure 35 Vertical Plane at Section 7. ..... A17
Figure 36 Vertical Plane at Section 8. ..... A18
Figure 37 Vertical Plane at Section 9. ..... A18
Figure 38 Horizontal plane at Z = 5.5 mTAW. A19
Figure 39 Horizontal plane at Z = 6.0 mTAW. A19
Figure 40 Horizontal plane at Z = 6.5 mTAW. A20

Figure 41 Horizontal plane at Z = 7.0 mTAW. A20
Figure 42 Horizontal plane at Z = 7.5 mTAW. A21
Figure 43 Vertical Plane at Section 1. ....A21
Figure 44 Vertical Plane at Section 2. ....A22
Figure 45 Vertical Plane at Section 3. ....A22
Figure 46 Vertical Plane at Section 4. ....A23
Figure 47 Vertical Plane at Section 5. ....A23
Figure 48 Vertical Plane at Section 6. ....A24
Figure 49 Vertical Plane at Section 7. ....A24
Figure 50 Vertical Plane at Section 8. ....A25
Figure 51 Vertical Plane at Section 9. ....A25

List of Tables

Table 1 Flow conditions of the tributaries (main channel, fish passage entrance) to the confluence. 8

Nomenclature

Abbreviations

CFD	Computational Fluid Dynamics
FH	Flanders Hydraulics
FOAM	Field Operation And Manipulation library
IMDC	International Maritime and Dredging Consultants
RAS	Reynolds-Averaged Simulation
VoF	Volume-of-Fluid

1 Introduction

The fishpass structure is a classical vertical-slot passage system, and adjacent to it an obermeyer-type sluice gate acting as a weir. Figure 1 shows a sketch of the fishpass and other features. There, discharge from the headwater upstream (called 'added discharge' hereinafter) from the sluice is added somewhere upstream from the entrance of the fish passage in an attempt to enhance fish attraction efficiency from the tailrace. The hydraulic design of this fish passage is described in Visser *et al.*, 2024, and the present numerical study will focus on the region highlighted in blue in Figure 1.

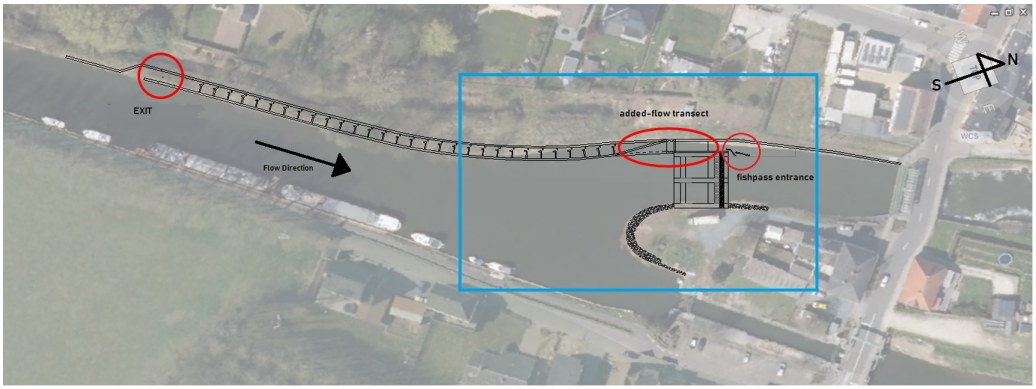

Figure 1 – Planview of the Denderleeuw lock in Dender. The highlighted regions in red indicate where study efforts have been made. The focus of the present computations are for the highlighted structure on the East (in blue).

In addition to the added discharge, a design for the fish passage entrance is also sought to improve attraction efficiency. Different alternatives for the added discharge in the so-called outflow channel (the channel section between the last vertical slot and the fish passage's entrance) was suggested and studied during the design phase for the fish passage in Merelbeke (Visser *et al.*, 2022). This first variant was investigated by means of CFD by Badano *et al.*, 2019 and based on their results it was determined that different alternatives needed to be proposed and further studied via CFD. These alternatives will be proposed also for the lock-weir complex of Denderleeuw, and supported by the present study using CFD.

1.1 Objectives

The objectives of the overall study, of which the present report makes part of, are the following:

- Guarantee an effective attraction flow at the fish passage's entrance, considering the effect of the weirs during their operation.
- Guarantee a migration corridor across the outlet channel, where the added discharge elements may be located.

Based on the aforementioned objectives, the primary focus of the present report is to provide insight on the effectiveness of the proposed structures in producing favourable attraction currents in the tailrace downstream of the weirs and within the approach channel to fish passage, based on the hydrodynamics obtained using CFD. But also, given the differences noticed between previous studies and the present, a secondary objective of the present work is to perform a critical assessment of the results obtained here in relation to previous studies.

Note that upon obtaining a satisfactory design of the structure providing admissible attraction currents in the

fish passage, the design will be replicated at other locations along the Dender namely: Idegem, Geraardsbergen, Pollare, Aalst and Denderbelle. However, in this report attention will be given to basic qualitative criteria for the assessment of fish attraction, and at the same time focus will be given to hydrodynamic and numerical aspects of the simulations. A final evaluation and verification of the design alternatives is out of the scope of the present work.

1.2 Fish attraction assessment criteria

The basic criteria used for assessing the performance of the structures, according to Visser *et al.*, 2024, is the following:

- Velocities approaching the entrance of the fish passage and within the fish passage should not exceed 1.5 m/s.
- Flow streamlines emanating from the fish passage's entrance should preferably be smooth (meaning little curvature) and extend as far as possible into the tailrace without hindrance.
- The flow from weirs should not introduce "excessive turbulence" to the flow near the fish passage entrance.

As it can be seen, these criteria are rather qualitative but may serve as a first insight into the simulation results. A more in-depth discussion on the passage performance will be done in further works.

1.3 Contents

Given that the present work focuses on two distinct elements of the fish passage, that is, the added flow in the outflow channel and the fish passage's entrance, this report will be split in two parts. The first part focuses on the modelling of the attraction flow towards the fish passage's entrance. The second part focuses on the modelling of the added flow in the outflow channel. Each part will contain descriptions and results made by Badano *et al.*, 2019 and those obtained in the present study, and conclusions summarizing the insights of the authors regarding the hydrodynamics and the fish attraction criteria therein. An additional chapter, included as an appendix, describes the effects of aeration on the present study and elucidates the reasons behind the differences found between the present study and the study of Badano *et al.*, 2019. Finally, recommendations for future research are suggested.

2 Simulation settings and preliminaries

This chapter will briefly describe the settings and boundary conditions used for the studies conducted by FH. The reader is referred to Badano *et al.* (2019) for the description of the simulation settings used by IMDC. Additionally, some basic parameters (eg. water depths, discharge) will be described for the cases that will be studied in this report.

2.1 Governing equations and turbulence model

The CFD algorithm and Reynolds-Averaged Simulation (RAS) model used for the present study is an in-house modification of the classical VoF model for two-phase flows of Ubbink and Issa (1999), and of the turbulence model of Menter and Egorov (2005) adapted for two-phase flows. The reader is referred to Castano *et al.* (2023) for details on the implementation and settings within Field Operation And Manipulation library (FOAM).

2.2 Boundary conditions and parameters

The present study will be conducted for hydrological periods corresponding to high-flows, that is, where the Dender river has a discharge with a 10% probability of exceedence. This corresponds to a discharge of 22.19 m^3/s, a water elevation of 10.37 mTAW upstream from the weirs, and a water elevation of 7.61 mTAW downstream from the weirs, according to Visser *et al.* (2024).

According to the designs conducted for the fish passage this structure was designed for a nominal discharge of 1 m^3/s for 10.37 mTAW upstream and 7.61 mTAW downstream. Various designs within the outlet channel have been proposed with the purpose of conveying an additional 4 m^3/s to the nominal flow of the fish passage, as it will be shown in upcoming sections. These structures may comprise open-water flow weirs or closed pipes under pressure.

At the time when the simulations by IMDC were conducted, the decision was made not to perform the simulations using the known discharge of the Dender river. Instead, the water level at each end of the channel was "fixed" by setting the hydrostatic pressure both at the inlet and the outlet. Although the study conducted by IMDC verifies that the discharge obtained by setting the upstream and downstream pressure is *roughly* similar to the exceedence discharge of 22.19 m^3/s (up to 27 m^3/s), the variability of the discharge in time is greater than the nominal flow through the fish passage (> 1 m^3/s), thus casting a degree of uncertainty over the *steadiness* of the simulations in relation to the added discharge and fish passage flow. It will be shown in later chapters that the unsteadiness of pressure boundary conditions can be non-negligible in some cases.

The *steady-state* simulations conducted by FH used Dirichlet boundary conditions for the inflow fluxes and *open* boundaries for the efflux, that is, the discharge is to be maintained constant at the inflow of the Dender river and the water depth is to be fixed at the outlet. This guarantees that all mass-defects are product of the discretization, and not due to unsteadiness originating at the boundary conditions nor to grid-dependence.

2.2.1 Adaptive Mesh Refinement (AMR) of Polyhedra

This section will present a brief description of what has been done to achieve adaptive mesh refinement for the current simulations. By default, FOAM only allows for octree AMR of hexahedral elements, that is, by splitting

a parallelepiped in four along its edges' bisectors. This condition is too limiting for complex meshes, generated by automatic meshing utilities, where hexahedra-dominant or fully hexahedrical meshes, with hanging nodes (by implication polyhedra), are commonplace. The Author has resorted to use polyhedral AMR, by implementing the necessary libraries (MESQUITE) onto the code and adapting them accordingly. Given the memory consumption of such procedure, it has been only used for the simulation described in Section 5.3.1.

Part I

Modelling of the attraction flow towards the fish passage's entrance

3 Previous CFD studies

The present chapter will briefly report on the results obtained by Badano *et al.* (2019) regarding the study of the attraction flow towards the entrance of the fish pass in the tailbay. The focus will be to highlight the most salient features of the flow for each of the scenarios studied.

3.1 Overview

For the study of the fishpass entrance, two different scenarios were considered for the added flow discharge Q_t during high-flow periods in the Dender channel. The discharge passing through the weirs Q_0 and the nominal discharge of the fish passage Q_v will be kept fixed during the simulations. Thus, the total discharge of the river equals

$$Q_{total} = Q_0 + Q_v + Q_t.$$

It is therefore assumed for the purposes of the present study that the three discharges are disjoint and each correspond to a different boundary condition. In reality water will be taken from the Dender river to feed the fish passage and the added flow, upstream from the weirs.

The main intent with the added flow in the fishpass is to reduce the difference between the incoming momenta from the fishpass and the main channel at the confluence, in order to have more favourable attraction currents towards the fishpass entrance. Additional guide vanes were proposed (Visser *et al.*, 2024) in order to provide escape to fish trapped in the flow within the left weir's plunge pool and to provide additional blockage to the flow coming from said weir. The geometry of the domain, and details on the weirs and guide vanes are shown in Figure 2. Note that geometric details of the downstream stilling basins (or buckets), the floor of the tailbay, and some other features of the weir were *simplified* since the final design of the structure was not finished at the moment of conducting this study.

As mentioned earlier, the ratio of incoming momenta to a confluence plays an important role in the understanding on whether one of the incoming currents is going to *overwhelm* the other. In other words, the ratio of momenta will help understanding whether the attraction flow from the fish passage will extend far downstream from the structure. The flux of momentum at the confluence from a tributary is defined as:

$$M = \rho Q U,$$

where U is the cross-section average velocity right before the confluence. The ratio of momenta for the present study is thus defined as:

$$r = \frac{M_0}{M_t + M_v} \tag{1}$$

$$= \frac{Q_0 U_0}{(Q_t + Q_v) U_{t+v}}. \tag{2}$$

Another parameter useful for this study is the Froude number:

$$Fr = U/\sqrt{gH}, \tag{3}$$

where g and H are the gravity and mean water depth, respectively.

The basic flow properties of the tributaries and relevant parameters for the two scenarios being studied (S2-A and S2-B) are described in Table 1. Note that for low added discharge case (S2-B) r is quite high compared to

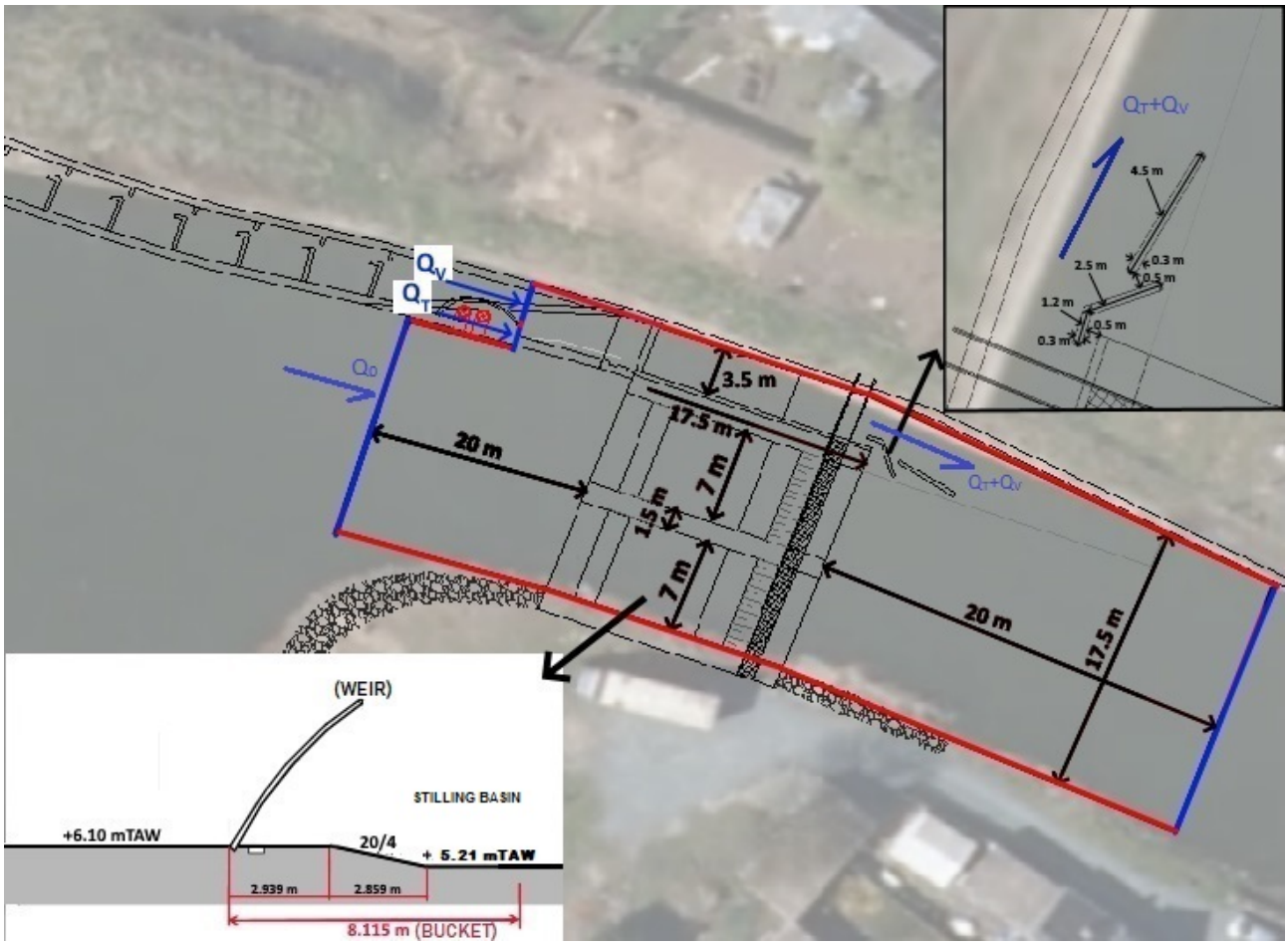

Figure 2 – Numerical domain considered for studying the attraction flow at the fishpass's entrance. The inlet/outlet boundaries are depicted in blue, the red lines depict the rest of the boundaries. Note that the added discharge (Q_t) and the nominal discharge of the fish pass (Q_v) have corresponding boundary conditions.

the high added discharge case (S2-A), thus it is expected that the attraction region after the fishpass entrance extends farther downstream in case S2-A. Additionally, the mismatch between the incoming Froude numbers is expected to produce small surface waves travelling upstream within the fish passage for case S2-B. Such assessments will be verified in the following sections.

3.2 Simulations conducted by IMDC

As indicated previously, two scenarios were studied by IMDC:

S2-A where a total of $Q_t + Q_v = 4\ \text{m}^3/\text{s}$ of added discharge in the fish pass is set on the rightmost inlet within the fishpass as depicted in Figure 2.

S2-B where a total of $Q_t + Q_v = 2\ \text{m}^3/\text{s}$ of added discharge in the fish pass is set on the rightmost inlet within the fishpass as depicted in Figure 2.

Both scenarios use $Q_v = 1\ \text{m}^3/\text{s}$ for the nominal discharge of the fish passage and $Q_0 = 20\ \text{m}^3/\text{s}$ for the flow in the main channel[1]. All dimensions are extracted from Figure 2. Note that none of the simulations considers the geometry of the added-flow accessories (the structures upstream of the blue line in the fish passage shown in Figure 2) in the topology of the domain, just a rectangular entrance with dimensions defined by the designer.

[1]The discharge with a 10% probability of exceedence was 22.19 m^3/s, but 20 m^3/s was chosen for the present simulations.

Table 1 – Flow conditions of the tributaries (main channel, fish passage entrance) to the confluence.

		Discharge [m^3/s]	U [m/s]	M [kg-m/s]	Fr [-]	r [-]
S2-A	Q_0	20	0.68	13575	0.14	9.05
	$Q_t + Q_v$	$3 + 1 = 4$	0.5	1500	0.10	
S2-B	Q_0	20	0.68	13575	0.14	20.35
	$Q_t + Q_v$	$1 + 1 = 2$	0.33	667	0.07	

For details on the simulation settings, geometry of the added-flow inlet, and solvers used the reader is referred to Badano *et al.* (2019).

3.2.1 S2-A case

The lower ratio of momenta in this scenario contributes to a larger attraction region downstream from the fish pass entrance with velocities not exceeding 1.5 m/s, as shown in Figure 3(a). Note there, however, that the jet coming from the leftmost weir expands slowly towards the left bank, constraining the flow there. The domain is not sufficiently long in order to be able to observe such constriction to happen. On the other hand, the added flow within the fish passage produces velocities well beyond the 1.5 m/s limit defined as criterium for the fish passability assessment.

Vertical planes of the flow along the domain are depicted in Figure 3(b). Note there that the flow velocities downstream of the weir, in the bucket, and downstream from the center pier also exceed the 1.5 m/s limit. High degrees of turbulence and, in particular, flow bulking are expected after the flow drop, further producing flow patterns that might be deterring or even harmful for fish. Aeration on the other hand seems rather weakened probably due to the drowned hydraulic jump after the flow drop. Additionally, the flow core seems to "lift" at the end of the stilling basin, indicating a weak adverse pressure gradient along the latter.

In general, the attraction flow produced downstream from the fishpass entrance can be beneficial for fish migration as fish might find a clear path in the tailbay that directs towards the fishpass's entrance. However, the flow within the fish passage and in certain regions of the tailbay might not be favourable for fish migration. However, this assessment may require a more in-depth study.

Finally, upon further verification of the total mass loss between the inlet and the outlet, the results confirm there is an *average* volume-rate loss of 1.31 m^3/s (two fifths of the fish passage flow, and 7% of the main channel inflow). Monitoring of the variations for this case is not feasible.

3.2.2 S2-B case

The increased momentum ratio r due to the reduction of the added discharge to 2 m^3/s leads to a weakened attraction flow towards the fish pass entrance, as shown in Figure 4(a). Regarding the guiding vanes it is clear at this point that their effect is marginal on the attraction flow, thus being r the major parameter driving the dynamics at the confluence of the domain.

Sections along the domain, depicted in Figure 4, show behaviour somewhat different to the previous case (S2-A) despite the fact that the flow and geometry upstream from the confluence remains practically unchanged. Note in particular the recirculation region trapped between the weir and the impinging jet: the roller seems more energetic (higher velocities within) for S2-A than for S2-B. Such discrepancy may indicate spurious transient effects being incorrectly averaged during the simulation.

In general, a preliminary assessment of the present simulation shows flow attraction patterns in the tailbay

that only partially improve from the previous case. More specifically, the flow exiting the fish passage for S2-B incurs in more curved flow patterns but seems slower compared to S2-A. In other words, the velocity fields in S2-B exiting the fish passage's entrance are now well below the 1.5 m/s limit but present stronger curvatures in their path.

Again, flow bulking seems weakened due to the weakened action of the surface roller after the impinging jet. Mass conservation errors, in the mean, amount to 1.14 m^3/s (one-fifth of the fish passage discharge, and 5% of the main channel discharge).

3.2.3 S2-A: verifications conducted by FH

Given the problems in mass conservation detected earlier, it was decided to conduct an additional simulation of scenario S2-A, and treat the boundary conditions as described in Chapter 2.2.

Some of the results obtained for simulation S2-A-FH are depicted in Figure 5. Note there a large separation region comprised by a bottom roller formed towards the end of the stilling basin towards the tailbay. The flow in the plunge pool "ejects" upwards, generating near-surface currents that enhance the main channel's integral momentum thus choking the flow coming from the fish passage's entrance. This sort of flow resembles that of flip buckets downstream of spillways. Also note that the velocity field near the free surface in the channel downstream is well above 1.5 m/s in an important section of the domain. Additionally it seems the increased mixing and turbulence generated at the impingement region of the jet in the "flip bucket" enhances the overall aeration and bulking in the downstream flow. Such bulking not only seem to enhance the surface roller formed by the seemingly drowned hydraulic jump just downstream from the weir, but it also produces a buoyant force in the air-water admixture that ends up ejecting the bottom flow jet *upwards* onto the free surface. This phenomenon is sometimes referred to as "white waters", and may extend far downstream from the source of aeration.

Regarding mass conservation errors, the present simulation reports a total error of about 0.05 m^3/s between the inlet and outlet of the domain.

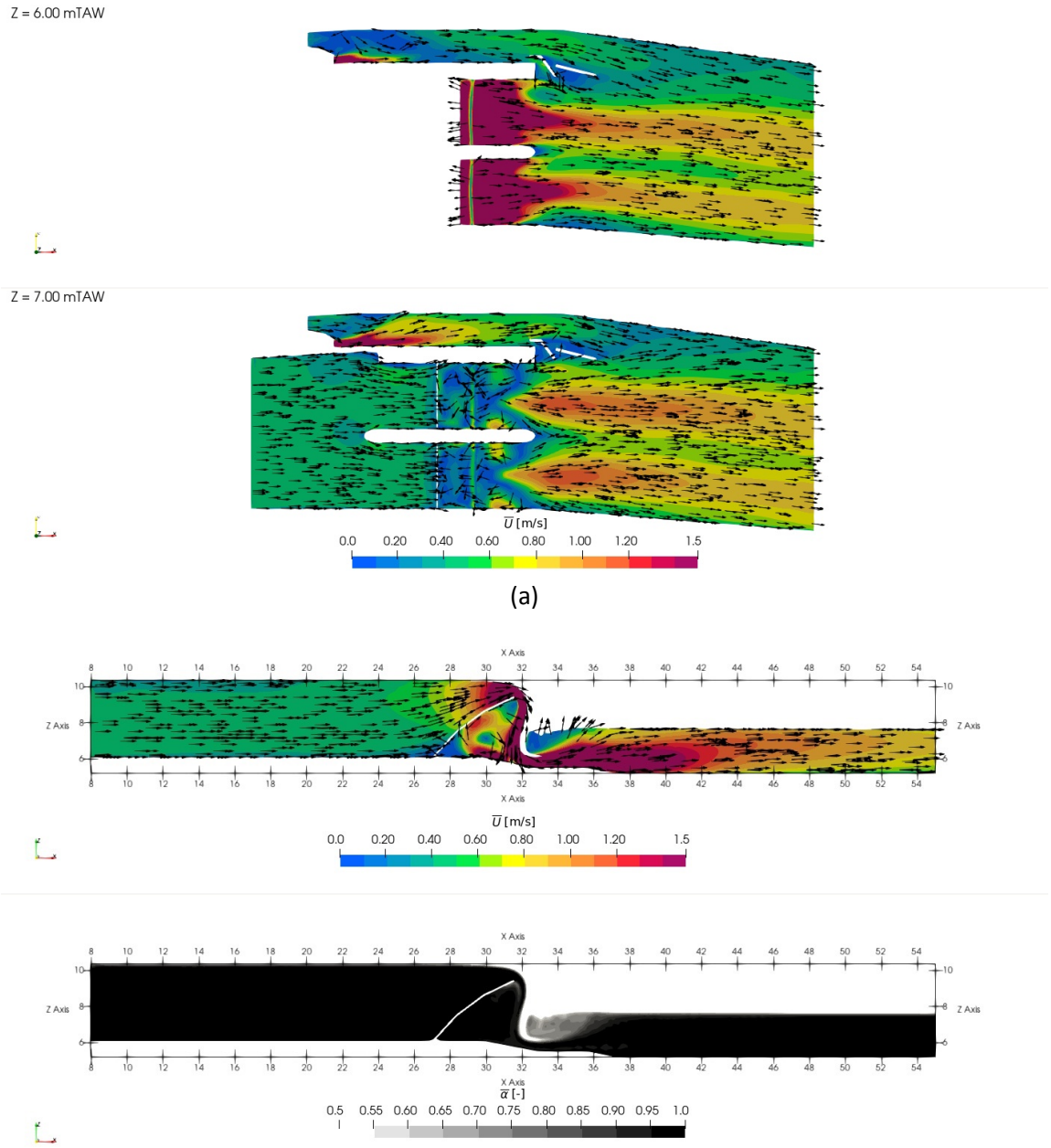

Figure 3 – Iso-contours of mean velocity and air-water phase-fraction for simulation S2-A, conducted by IMDC. The origin of coordinates is chosen arbitrarily for the horizontal axes.

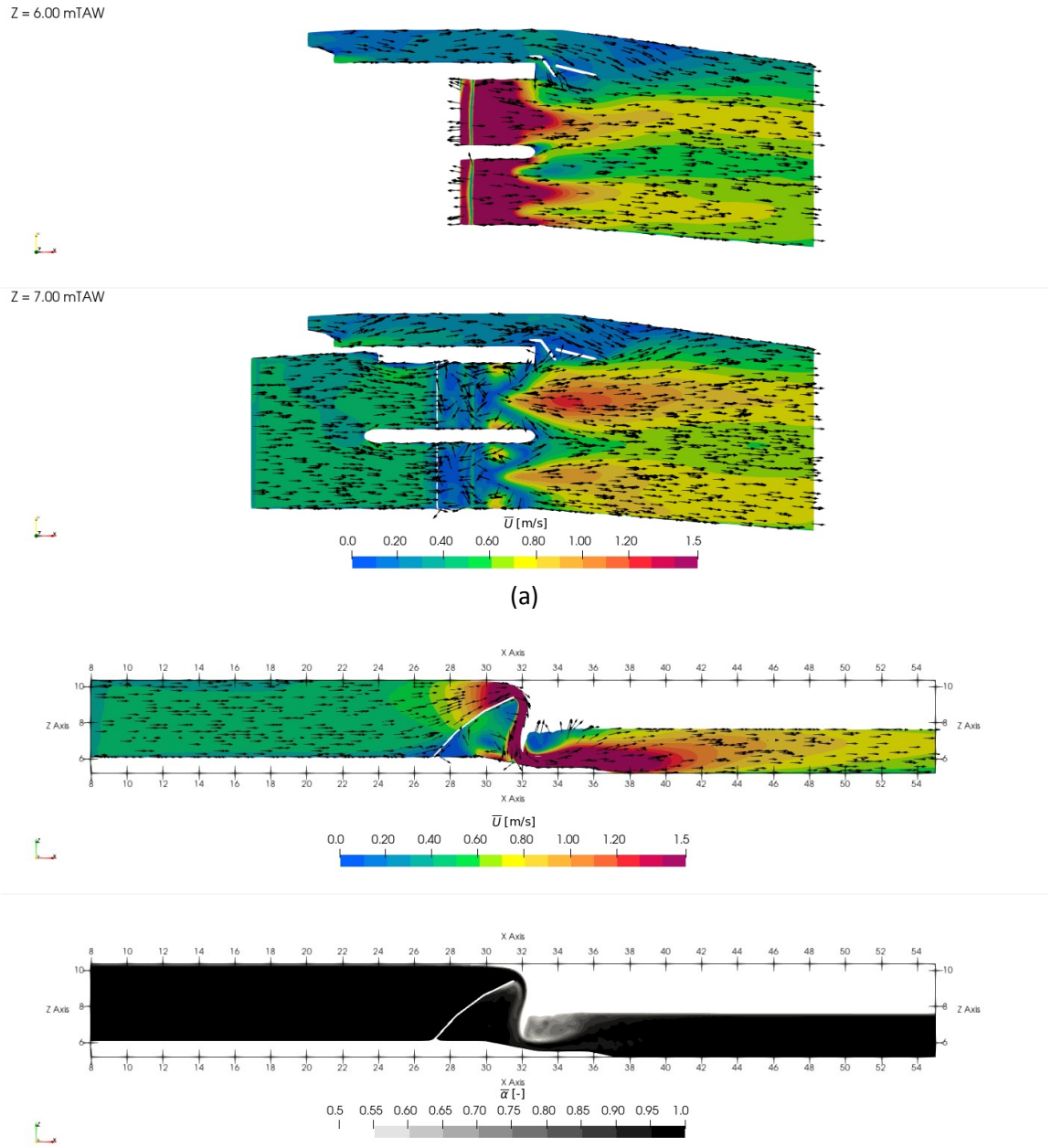

Figure 4 – Iso-contours of mean velocity and mass phase-fraction for simulation S2-B, conducted by IMDC.

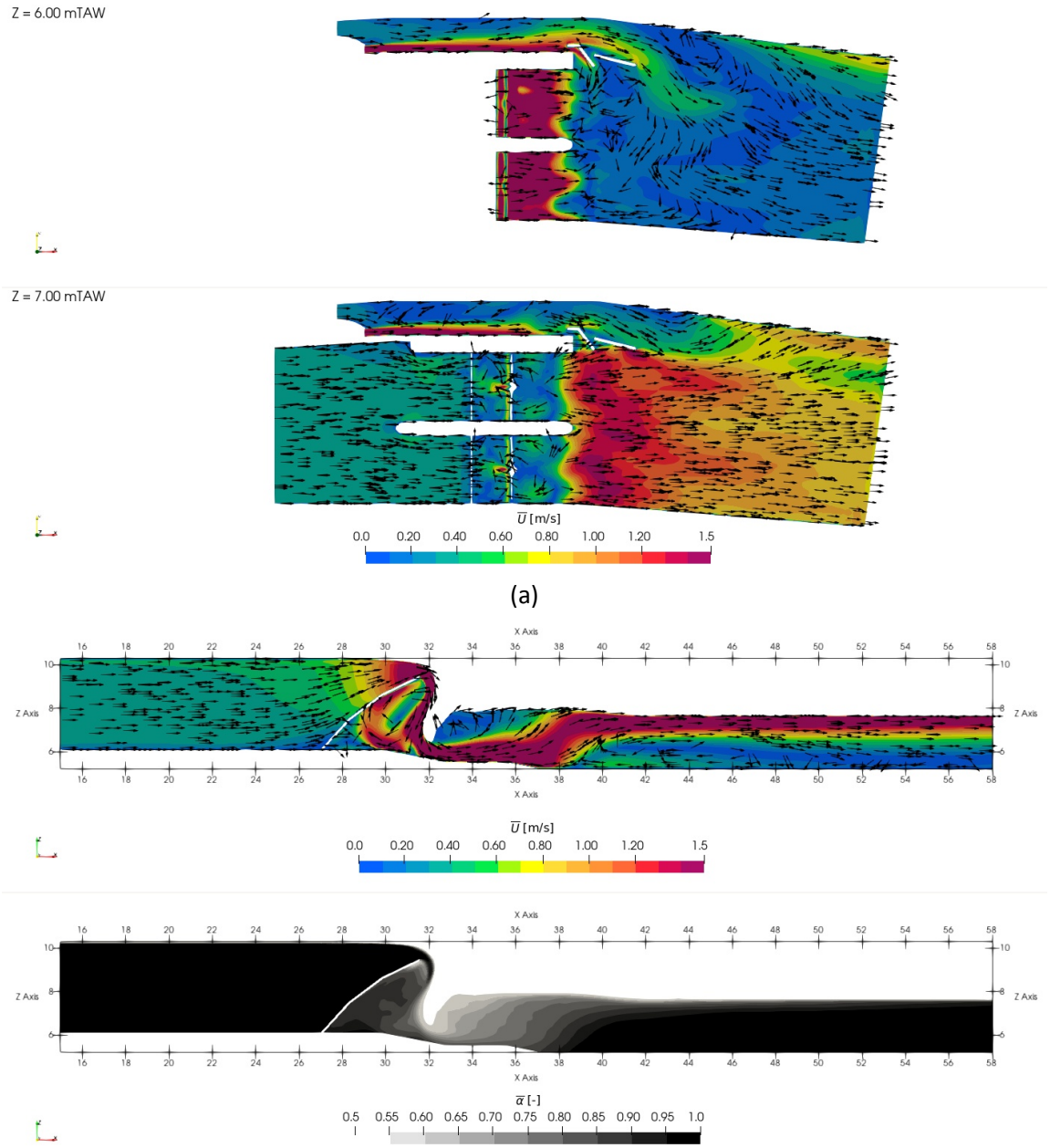

Figure 5 – Iso-contours of mean velocity and mass phase-fraction for simulation S2-A, conducted by FH.

4 Simulations conducted by FH

Some time after the study of Badano *et al.* (2019) was conducted, the following changes to the geometry of the domain were proposed:

- The dimensions of the center pier and of the spilling basins are corrected to the latest design.
- Nappe breakers at the weirs were introduced in the domain, following some general descriptions found in the designs. These were introduced in the simulations in order to avoid the impinging jet to attach to the weir's back wall (e. g.: see Figure 3).

With the aforementioned modifications, two scenarios were considered. First, a "Baseline" case with a tailbay channel with no guide vanes at the fish passage's entrance. Second, an "Alternative 1" case including guide vanes, and a channel contraption at the confluence between the fish passage's entrance and the tailbay which is straightened downstream. The dimensions and location relative to the fish passage's entrance of the guide vanes are the same as the ones studied by Badano *et al.*, 2019. The geometry of both scenarios are shown in Figure 6.

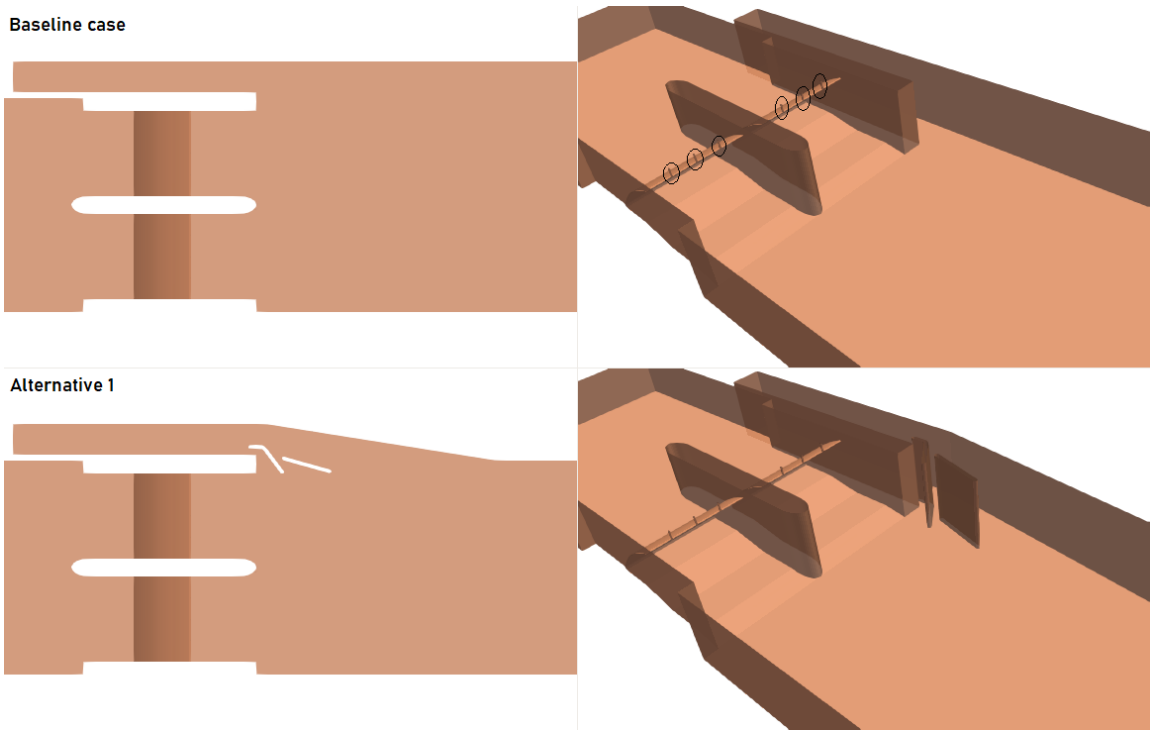

Figure 6 – Geometry of the main channel and fish passage entrance for the simulations conducted by FH. Note the baseline case includes no vanes, while alternative 1 includes vanes and a side-wall contraction at the left bank.

Note that all scenarios use $Q_v = 1$ m^3/s for the nominal discharge of the fish passage and $Q_0 = 22.16$ m^3/s for the flow in the main channel. Furthermore, in an attempt to make the analysis of the added flow in the fish passage (see Section 5.1) consistent with the study of the attraction flow in the tailrace, the added discharge to be used will be either $Q_t = 2$ m^3/s or $Q_t = 4$ m^3/s. This is a departure from the studies conducted by IMDC, where different Q_t and Q_0 were used. Here, only low added-flow discharge ($Q_t = 2$ m^3/s) results are shown.

4.1 Baseline case

The baseline case, shown in Figure 6, exhibits flow patterns that resemble those obtained already in simulation S2-A –conducted by FH. Results shown in Figure 7 depict two recirculation patterns, one surface roller produced by the drowned hydraulic jump and another bottom roller produced by the de-gassing of an initially *bulked* flow, that hinder the attraction flow towards the fishpass entrance. This phenomenon is particularly strong in the first 1.5 m of the water column, producing counter-currents which lower the pressure locally and lead ultimately to the attraction flow being sucked into the left bucket, as it can be observed in more detail in Figure 7(a).

Note also that a strong surface current forms downstream of the weirs and extends for around 10 m in the main channel. It is clear from previous analyses that such current might be detrimental to fish migration, however a more in-depth discussion may need to be held in such respect. This phenomenon is commonly referred to as "white waters" or outwash[2].

Finally, the effect of the nappe breakers is evident: an air pocket with pressures equal to the atmospheric is formed below the weirs. Such air pockets guarantee the detachment of the "vena contracta" from the weir, producing a more natural jet that impinges the pool downstream. Also that the bulking represented by α in Figure 7(b) is somewhat lower to that in Figure 5(b), probably due to the ventilation guaranteed by the nappe breakers.

4.2 Alternative with vanes and confluence contraction

The case referred to as "Alternative 1" in Figure 6 exhibits some improvements regarding the overall flow hydrodynamics and in particular the flow attraction towards the fishpass, as depicted in Figure 8. Note that the flow contraction produced both by the slanting of the left bank and the blockage produced by the guide vanes lead to a local increase of momentum and effective disconnection between low-pressure regions and the attraction flow itself, see Figure 8(a). The bulking and de-gassing phenomenon leading to the bottom rollers is still strongly present and produce high surface velocities in the upper 1 m in the water column.

4.3 Concluding Remarks

In general, the discrepancies between the simulations conducted by FH and IMDC are quite remarkable. The former seems to present more *chaotic* (as in more recirculations) flow patterns and overall velocity fields, along with increased bulking, while the latter exhibits flow patterns more familiar to un-aerated flows but tend to under-predict features such as self-aeration and the length of the surface roller after the hydraulic jump. The question that remains is whether the discrepancies seen here are due to over-dissipation, unsteadiness produced by the boundary conditions, or incorrect accounting of the physical drivers producing such flows.

The question of simulation unsteadiness cannot be assessed for the studies conducted by IMDC without repeating all of their simulations, which is not feasible at this point. Only strict mass conservation can be proven for the simulations conducted by FH.

A discussion will be held in Appendix A1 where the mechanisms that lead to enhanced losses and the appearance of additional bottom rollers in aerated flows are thoroughly explained. There, it is shown that the flow features seen in *all* simulations, the present or previous, may be explained just by the degree of self-aeration (or lack thereof) being resolved during the simulations.

[2] Sailors in fluvial waters and kayakers in particular are quite familiar with those terms.

In general, the simulations conducted by FH show that under high-flow conditions the alternative presented in Section 4.2 seems to have the most favourable flow attraction features of all designs being proposed. Furthermore, these alternative include the effects of a flow bulking and subsequent bottom recirculations in the solution. Note that this conclusion contradicts the previous findings made using IMDC's results, where the solution with guide vanes didn't seem to improve fish attraction efficiency.

It is however of fundamental importance for the simulations to be conducted using a more realistic geometry of the weirs and of all (hydraulically relevant) other appurtenances attached to the structure; as it has been shown, accessories such as nappe breakers can have a non-negligible impact in the overall hydraulic performance of the structure. Note that all simulations conducted so far are missing the bladder that operates the Obermeyer weir.

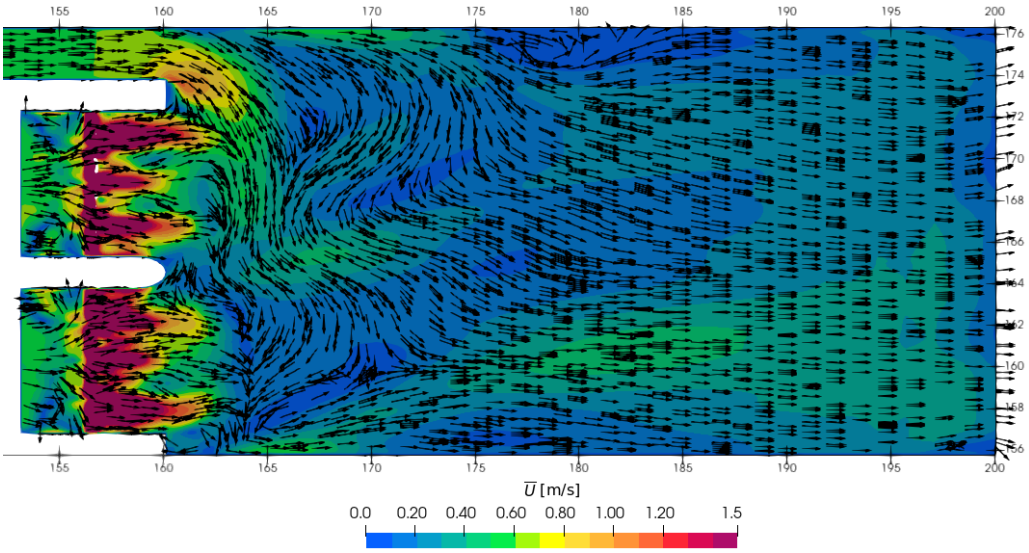

(a) Z = 6.00 mTAW

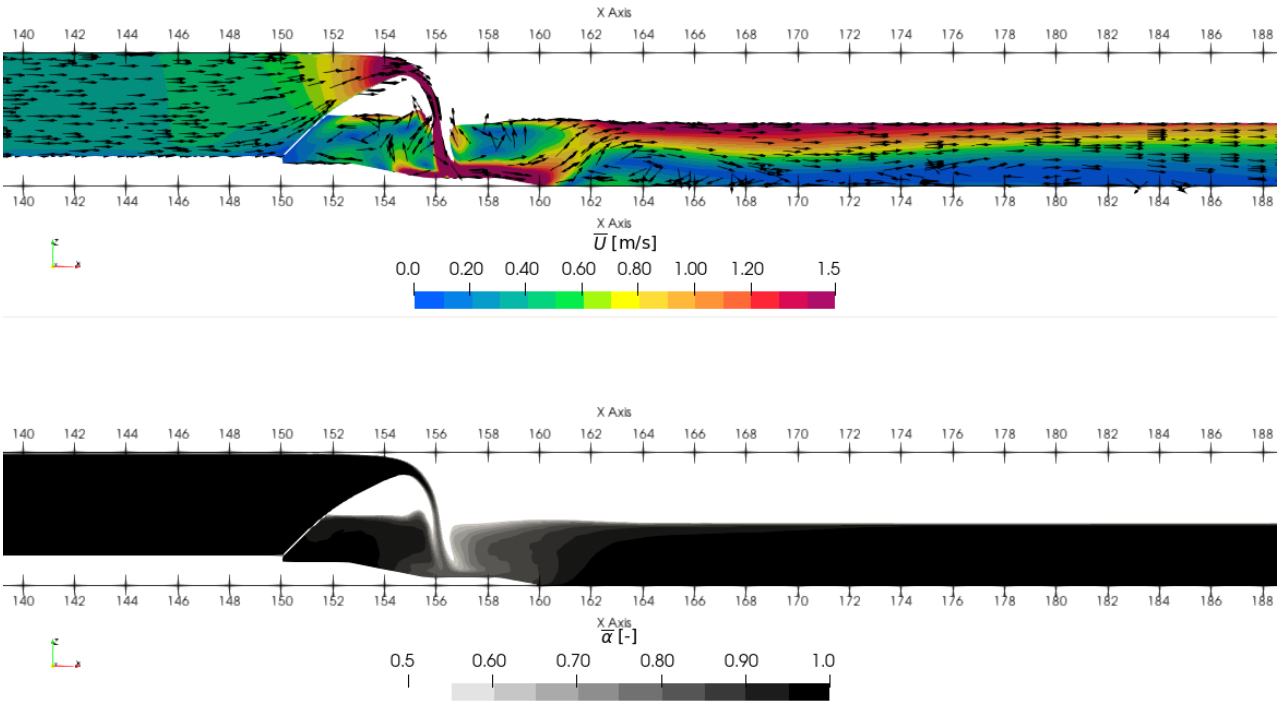

(b) Y = - 9.00 m

Figure 7 – Results obtained for the baseline simulation conducted by FH.

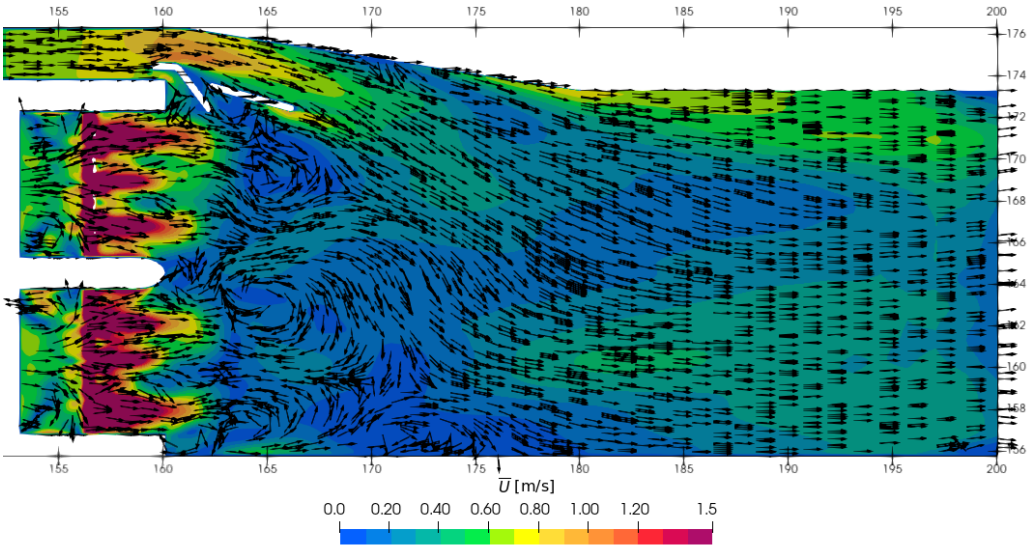

(a) Z = 6.00 mTAW

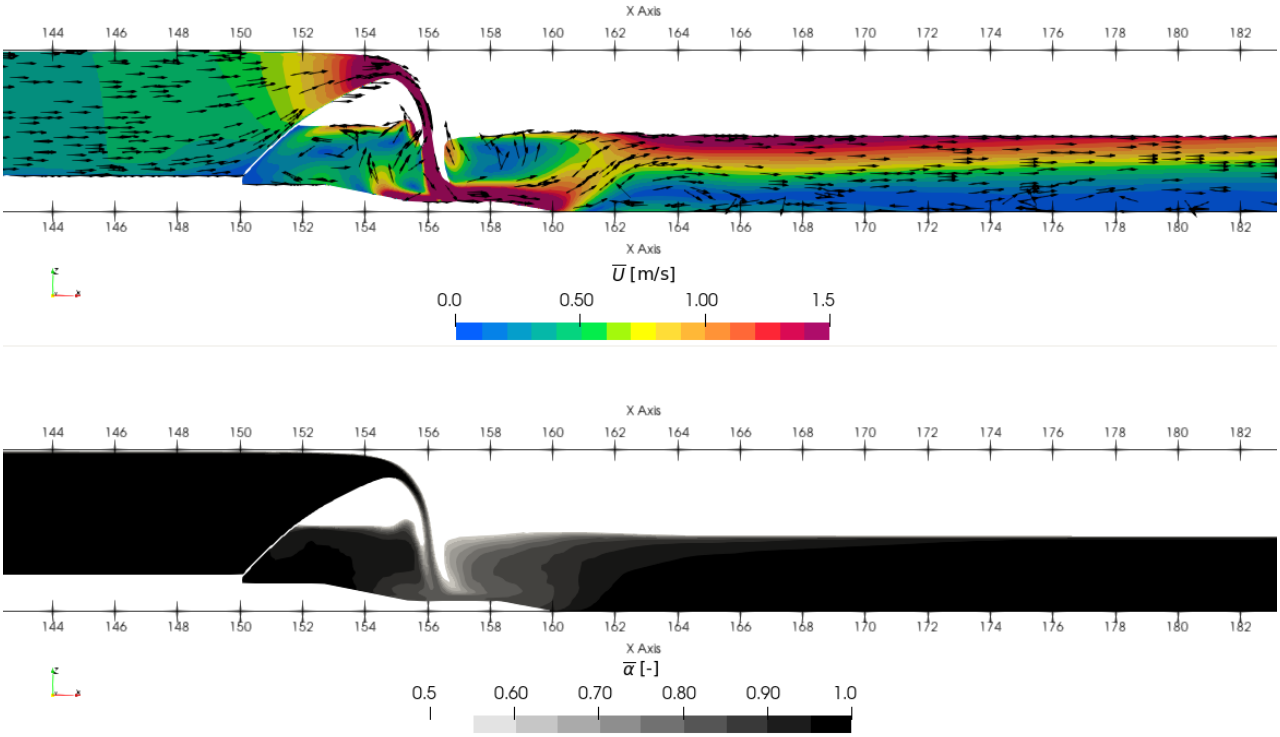

(b) Y = - 9.00 m

Figure 8 – Results obtained for the baseline simulation conducted by FH.

Part II

Modelling of the added flow in the outflow channel

5 CFD studies

5.1 General

Two basic strategies have been proposed to improve the attraction current at the entrance of the fish passage:

- Added flow through **pipes in a basin**, controlled by a valve: The added flow rate is introduced through two pipes into a basin located in the transect connecting the fishpass entrance with the vertical-slot channel. Figure 9(a) shows the location where the added flow is introduced into the fish passage. The pipes are equipped with a gate or valve to be able to close them or to regulate the flow through these pipes.
- Added flow through a **submerged gate** from the forebay: The added flow is conveyed from the forebay to the fish passage via a lateral intake with a lift gate. The flow from the fish passage itself is led downwards across a submerged culvert. Figures 9(b) and 9(c) shows a top view and a cross-section of the sleeve for introducing the added flow rate. A knife gate is provided in the upper tube to be able to interrupt or control the flow.

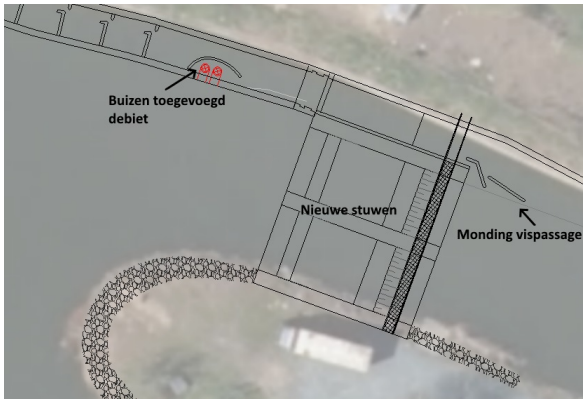

(a) Pipe-basin couple.

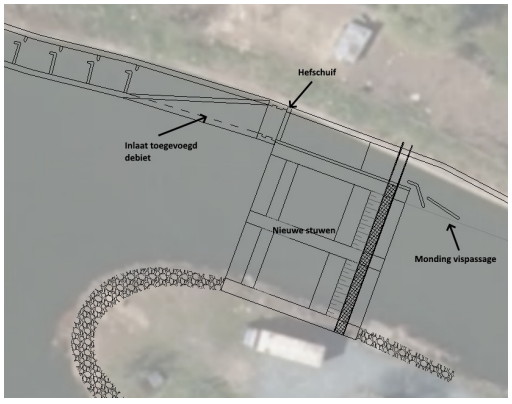

(b) Top view submerged slanted gate.

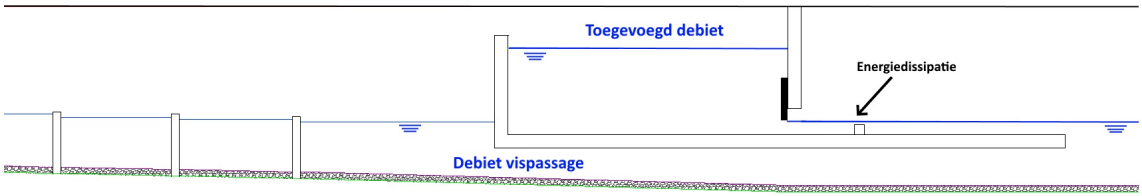

(b) Side view submerged slanted gate.

Figure 9 – Fish pass outflow and added flow alternatives proposed by Visser *et al.* (2024).

5.2 Simulations conducted by IMDC

Adding vanes were already explored in previous chapters, which were placed downstream of the fish passage's entrance in an attempt to direct the flow away from the weir's. There, the desired effect of the vanes was relatively marginal in relation to the ratio of momenta present at the confluence. Here, however, the relation

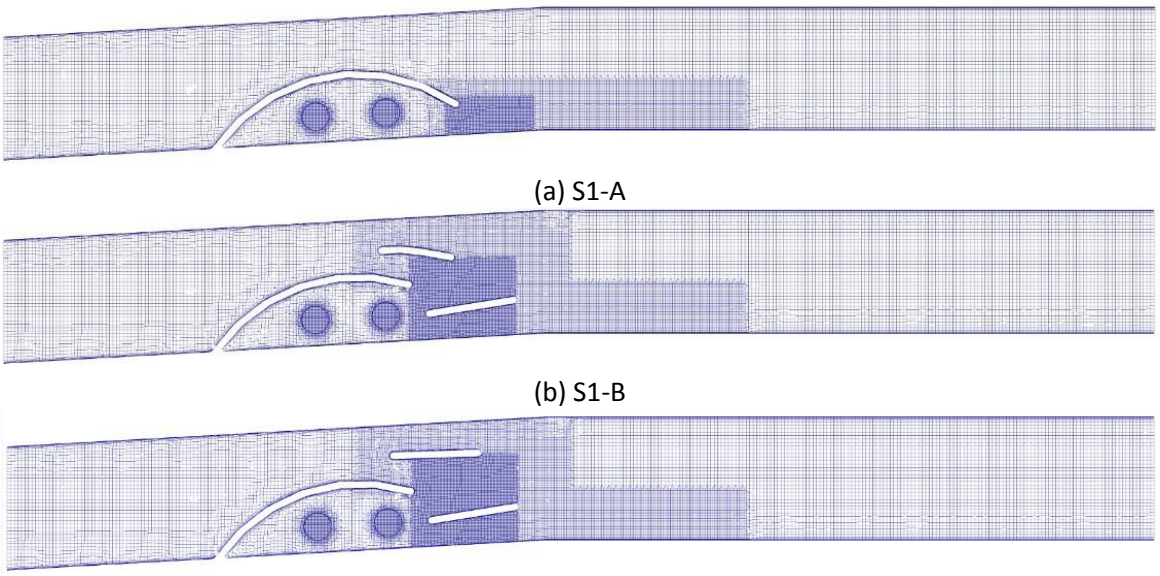

(a) S1-A

(b) S1-B

(b) S1-C

Figure 10 – Mesh topology and guide vane configurations proposed in Badano *et al.* (2019).

between the nominal discharge and the added discharge is kept roughly similar, hence suggesting that the guide vanes may prove more effective.

At this stage, an in-depth analysis of the basic geometry proposed in Figure 9(a) for the fish passage outlet was performed by IMDC. The added flow alternative using submerged gates was not considered therein. As explained earlier, the nominal discharge from the vertical slots is kept at 1 m^3/s, while two added discharge quantities are used: (a) 2 m^3/s, and (b) 4 m^3/s. The study performed by IMDC, however, only conducted simulations for the highest added discharge. Finally, three different guide vane configurations were considered:

S1-A No guide vanes.

S1-B Two vane configuration.

S1-C Two vane configuration with longer vane.

The topology of the domain and different vane configurations are shown in Figure 10. Details on the design and dimension of the vanes may be found in Visser *et al.* (2024).

The simulations conducted by IMDC only comprise the added discharge through the pipes in a basin placed within the outflow channel. There, three variants were proposed: a design with no guide vanes at the outlet of the basin, and then two other variants with vanes. The decision of adding vanes stems from the solution obtained from the first variant.

The present section discusses first the initial variant, with no vanes. Based on that discussion, reasons for pursuing the following two variants will be made. This section closes with a discussion providing the reasons for considering different alternatives, explored further in the following chapters.

5.2.1 S1-A: No guide vanes

Results for the first variant, as initially proposed, are shown in Figure 11. Notice that the design includes a small step within the dissipation basin. This step is meant to represent the difference in bed material within the basin and the channel. The bed within the basin is going to be covered in riprap.

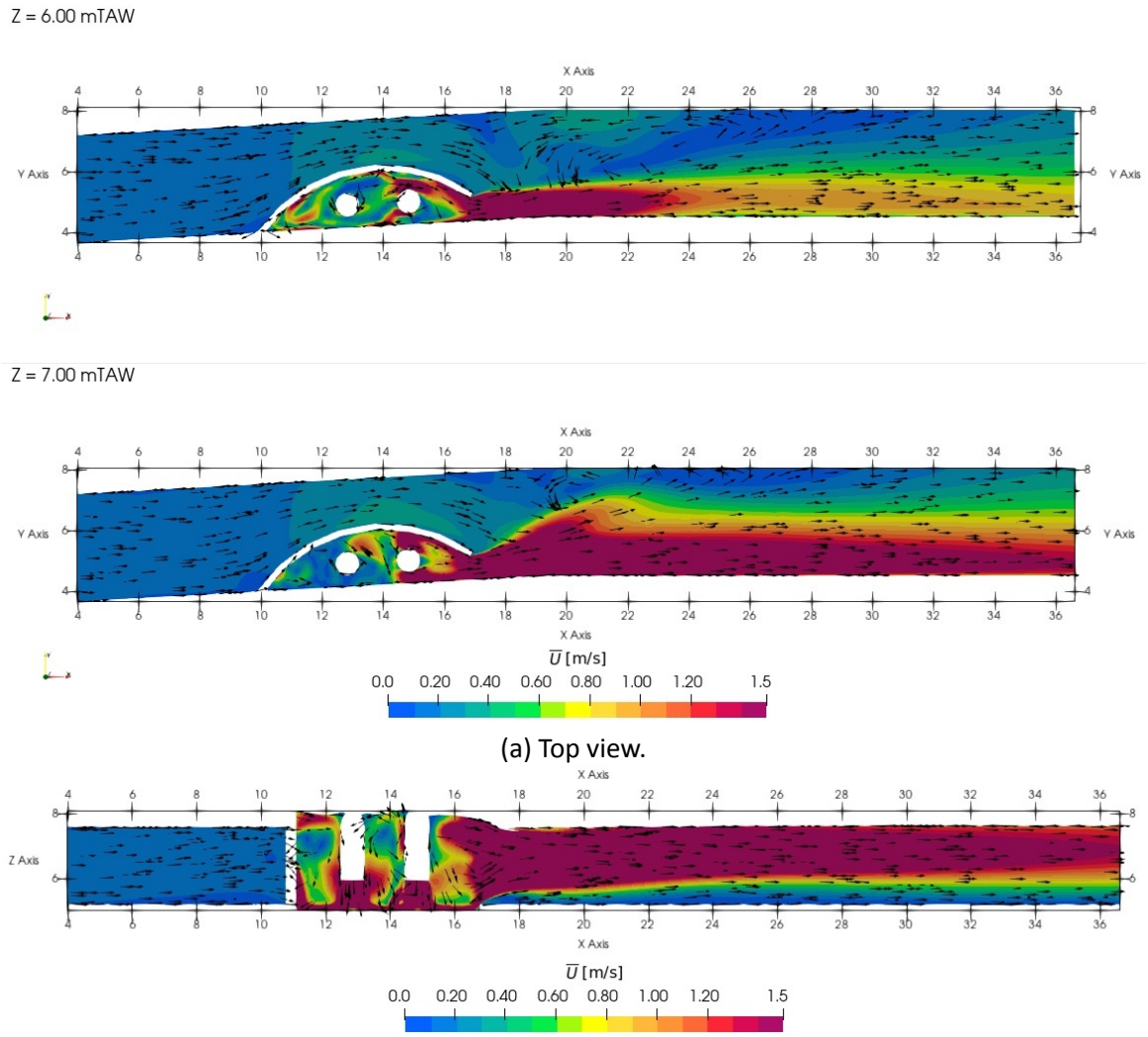

(a) Top view.

(b) Side view, Y = 5.00 m.

Figure 11 – Simulation results for the S1-A case run by Badano *et al.* (2019).

The numerical results show, however, that the proposed design introduces features onto the flow that might not be desirable from a point of view of fish swimming paths. Figure 11(a) illustrates the aforementioned statement more clearly. More precisely, the combined effect of the sill and the aforementioned jet is the formation of a lateral recirculation at X=20 m onward. Note that closer to the bed, Figure 11(b) shows a relatively strong jet, with velocities ranging from 0.8 to 2.0 m/s, coming out of the basin. Such jet seems to persist up to the outlet of the domain, which corresponds to the entrance of the fish passage. The design constraint mentioned earlier suggest that such high velocities may be counter-productive in attracting fish. Additionally, the rather narrow outlet from the pipe-basin increases the overall momentum ratio of the flow at the confluence with the nominal discharge, thus promoting the large recirculation region at the confluence downstream of the basin. Note that the step in the basin directs the core of the added flow towards the free surface, hence producing increased velocities in the upper half of the water column downstream. This vertical motion promotes some degree of mixing between the flows that meet at the confluence. However, such increased mixing is ineffective in *dissipating* the incoming kinetic energy from the basin.

5.2.2 S1-B and S1-C: guide vanes

Figures 12 and 13 show what is supposed to be an improvement from the previous variant, by adding guide vanes at the outlet of the pipe-basin system. It is assumed that the vanes will somehow disrupt the formation of the recirculation region downstream of the basin by moving the confluence between the flows further downstream while "concentrating" the outgoing jet towards the fishpass entrance. Additionally, the outlet of the basin is made wider, while allowing for an additional vane to split the projected jet from the bottom to the core of the water column.

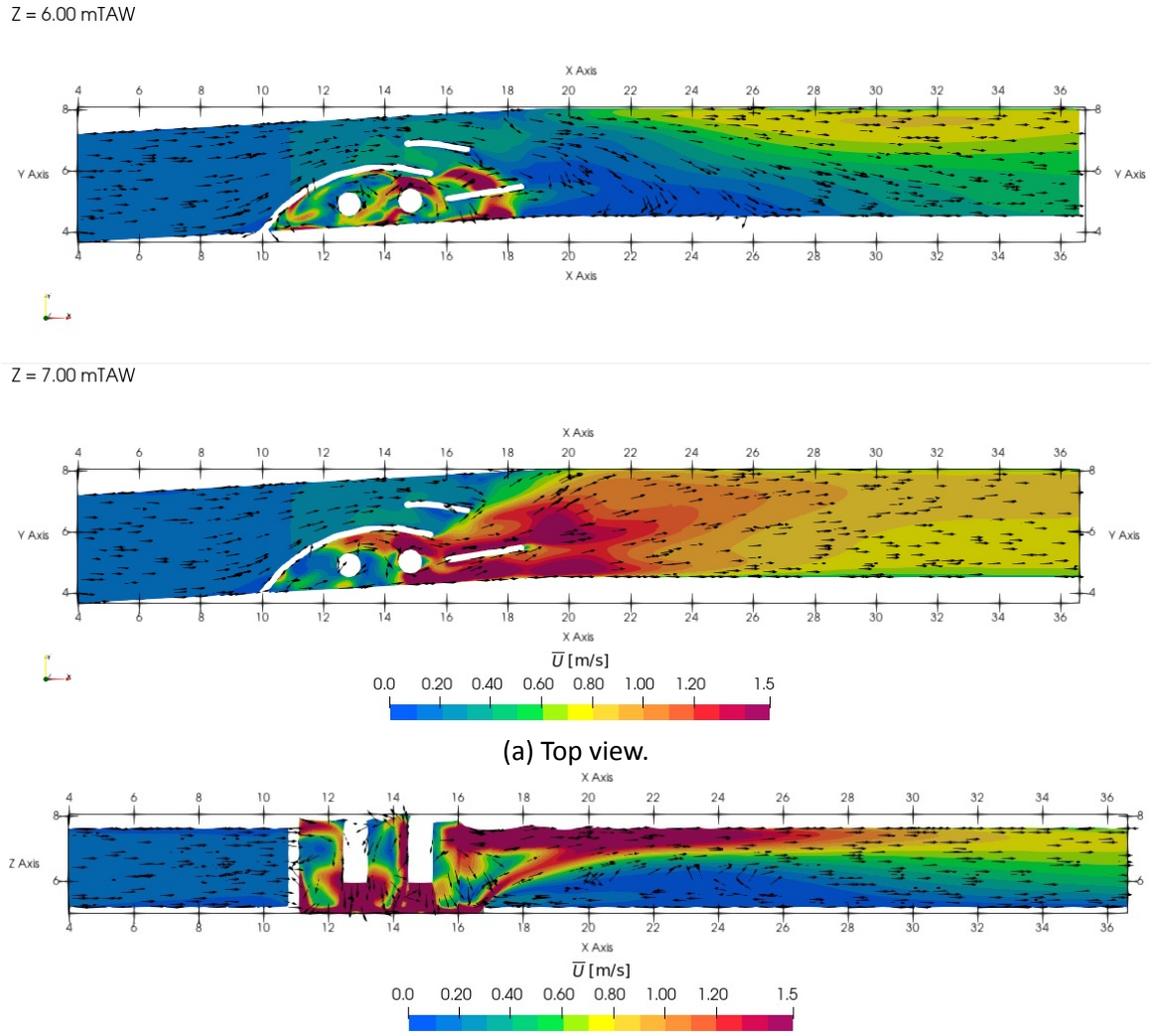

(a) Top view.

(b) Side view, Y = 5.00 m.

Figure 12 – Simulation results for the S1-B case run by Badano *et al.* (2019).

The different plane sections depicted in Figures 12(a) and 13 (a) show, in a qualitative manner, the flow features that were expected from the modifications just proposed. Note that by opening the outlet of the basin and placing a guide vane in the middle of it, the added flow is guaranteed to pervade the whole channel width. However, velocities continue to be rather high near the outlet of the domain. Note also that the guide vane closer to the left bank generates a return flow from the incoming jet, as it impinges directly onto the jet. Additionally, the step in the basin strengthens the bottom-to-surface jet produced by the added flow. Such jet induces a rather large recirculation region (or separation bubble) that encompasses more than half of the water column, for a long stretch of the downstream channel. It is difficult to determine whether the latter feature would have a strong effect on fish swimming within the fish passage. However, the rather high velocities near the step suggest strong erosive forces could be acting there, calling for measures that may prove costly, given

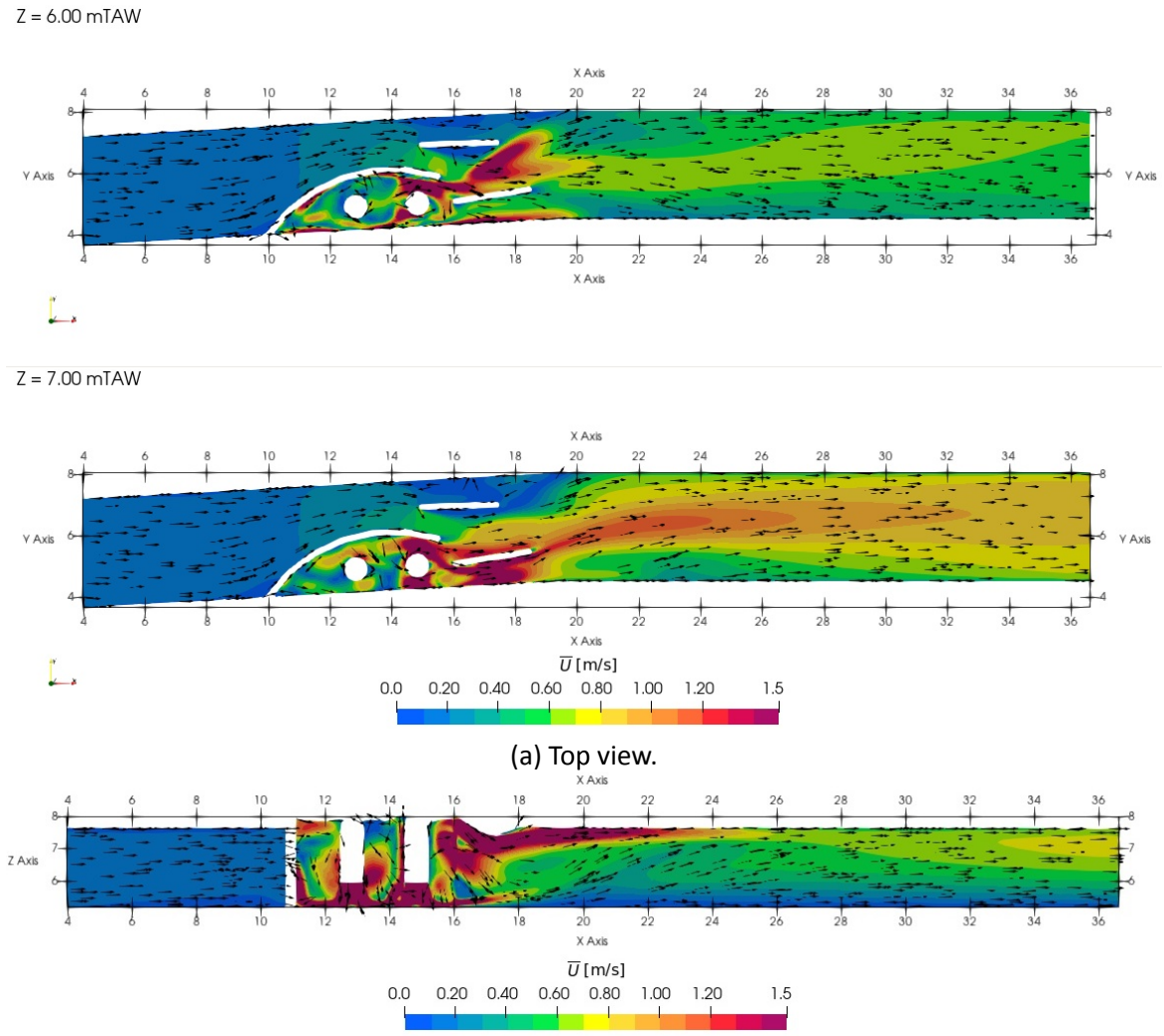

(a) Top view.

(b) Side view, Y = 5.00 m.

Figure 13 – Simulation results for the S1-C case run by Badano *et al.* (2019).

the undesired effects of having the step in the first place. In fact, the removal of the positive step in simulation S2-C (see Figure 13 (b)) proves to have a marginal effect in the hydrodynamics downstream when compared to case S1-B (see Figure 12 (b)).

5.3 Simulations conducted by FH

As mentioned in previous sections, the studies conducted by IMDC were limited to a certain added discharge and certain geometry, more precisely the pipe-basin system. The results obtained there proved that the positive step in the basin is deleterious for the flow downstream of the basin but also the configuration of the basin itself has negative effects, thus it is not clear whether just by removing said step an overall improvement will be seen for case S1-A and following cases. Furthermore, by placing all the added discharge on a single basin seems to produce excessive velocities downstream of the basin. This leads to think of an alternative where the added discharge is distributed amongst more than one basin, in order to reduce the incoming momentum from each basin.

A new design correcting all the flaws perceived in the previous studies was proposed , and modelled herein. For completeness, all alternatives proposed (including the present) by Visser *et al.* (2024) are also studied using

CFD.

5.3.1 Added flow: Submerged slanted intake

The alternatives for added flow start from the assumption that water can be drawn from the Dender channel and funnelled to the fish passage in order to improve the attraction efficiency of the latter. Instead of using a system where water is pumped through pipes towards the fish passage, one may alternatively draw water directly from the forebay by placing a a lateral intake regulated using a knife gate, as shown Figure 9(b).

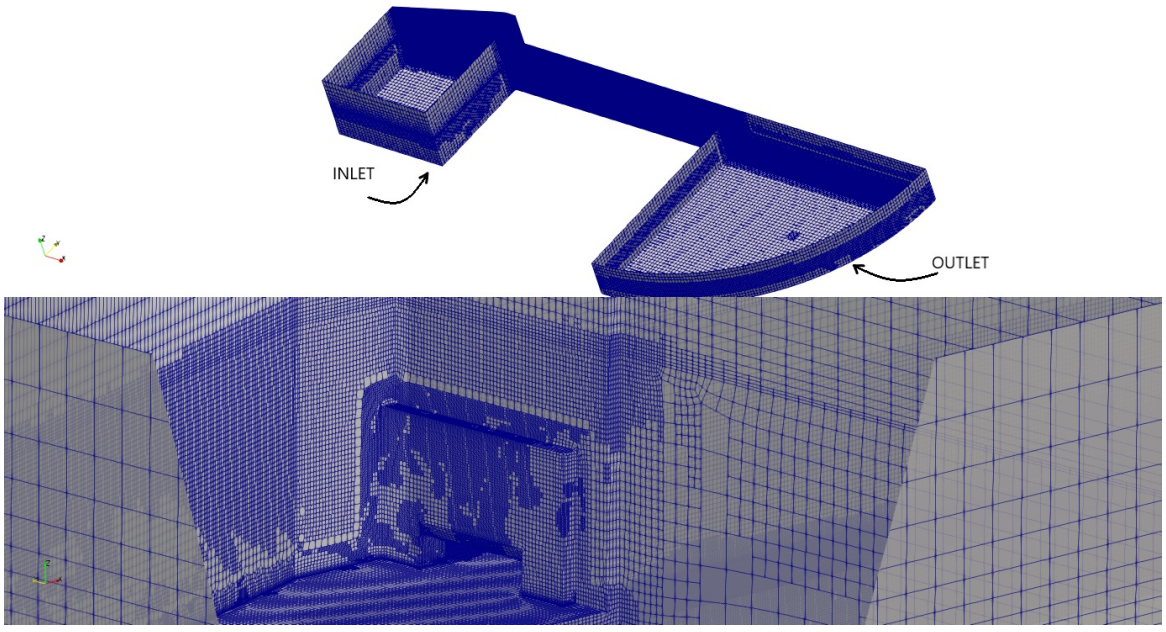

(a) Geometry and topology of the mesh (notice the use of AMR).

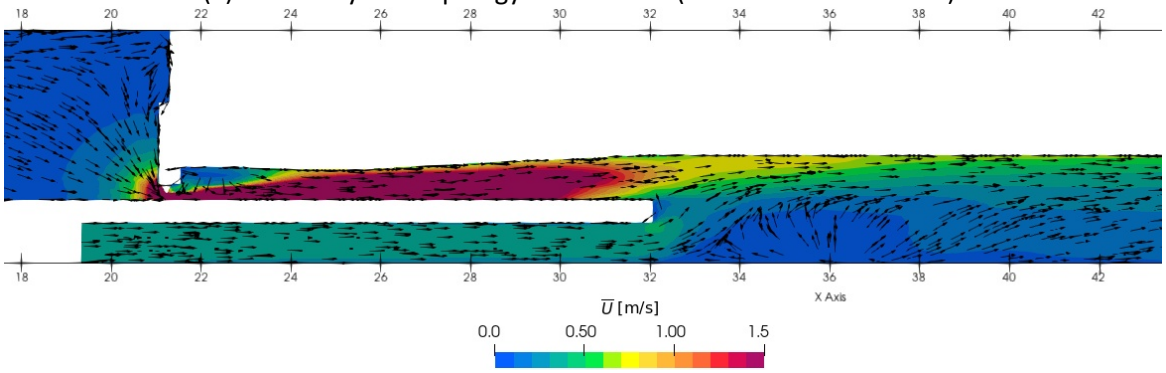

(b) Section along the middle of the submerged gate.

Figure 14 – Submerged slanted intake case.

The geometry and topology of the domain is somewhat complex, as it can be seen in Figure 14(a). Since the discharge is regulated by the knife gate's opening, the upstream boundary condition on the forebay cannot be a fixed discharge if one is interested in verifying the opening law of the gate. Hence, similar to what IMDC did for the studies involving the attraction flow towards the fishpass, the upstream boundary condition is set to have fixed hydrostatic pressure instead of fixed mass flux and the gate opening[3] is set to allow a theoretical added flow of

$$Q_{\text{gate}} = C_d\sqrt{2gH}A_{\text{gate}} = 0.61 \times \sqrt{2g \times (2.73)} \times (0.21) \approx 0.943\ \text{m}^3/s,$$

[3]The gate opening was set to be 14 cm and a width of 1.5 m.

where A_{gate} and H are the knife gate's opening area and the height difference before and after the gate, respectively.

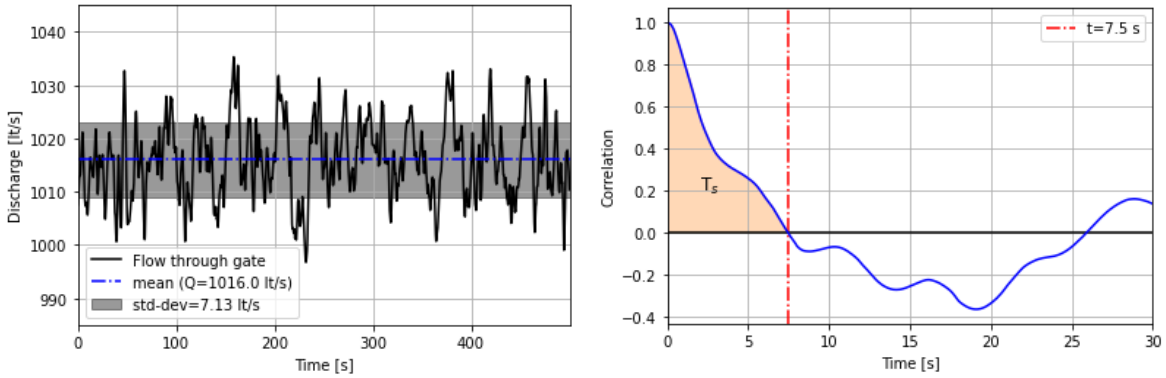

(a) Discharge through knife gate.

(b) Time auto-correlation of the flow discharge.

Figure 15 – Unsteadiness of the flow through the knife gate.

Before moving to the results, a time series of the discharge crossing the knife gate opening is shown in Figure 15(a). Said discharge is not steady, given the transient nature of the boundary conditions used in the present simulation, therefore a verification of the simulation's *steadiness* is needed. The mean discharge obtained from the time series is around 1.02 m^3/s, which is slightly higher compared to the expected added discharge Q_{gate} but still within the standard deviation and less than 10% difference that is typically allowed in hydraulic engineering studies. However, the discharge's time series is not *ergodic*, that is, the time correlation of the discharge through the knife gate doesn't fall off stochastically thus implying non-steady behaviour (see Figure 15(b)). In fact, the integral time scale of the auto-correlation for the discharge through the gate is equal to

$$T_s \approx 3\ s.$$

This integral time scale indicates the time lag across variations around the mean discharge; in steady flows, said time lag must be zero[4] since no variations exist. In unsteady computations of steady flows, the time lag should be of the order of the *time step* for ergodic fields; in the present case, the simulation was run with a fixed time step of 0.125 s.

One may conclude for the present analysis that although the assumption of ergodicity cannot be strictly assumed for the averaged fields obtained in this case (for time-dependent fields, that is), however the variations in discharge are so small that might have little effect on the outcome (or the mean fields).

That being said the results shown in Figure 14(b) reveal that this alternative is not feasible anyway, for various reasons: (1) the velocities in the upper concrete slab downstream of the gate are too high and may lead to erosion, (2) supercritical velocities higher than 5 m/s are bound to generate vibrations in the knife gate, (3) velocities higher than 3 m/s are bound to generate flow bulking, and (4) there is a strong backflow region forming at the confluence between the two tributaries. Because of this, analysis of the present alternative will not be pursued any further.

5.3.2 Added flow: two basins and contraction

The remaining alternative to explore is the pipe-basin system. Unlike the geometries studied by IMDC, here it is proposed to use two alternating pipe-basin inflows for the added flow. An additional contraction after the basins is suggested, in an attempt to increase the overall momentum of the flow at the outlet of the domain and reduce the chance of a recirculation forming at the confluence between the last basin and the fish passage

[4] In reality, for turbulent flows, this time scale should be of the order of the dissipative (Kolmogorov or Taylor) time scale.

flow. In addition to the aforementioned improvements in the design, it was decided to also add a more realistic inlet representing the outflow from the vertical-slot passage. The proposed geometry and mesh are shown in Figure 16.

Simulations were conducted for added flows of 2 m^3/s (low) and 4 m^3/s (high) and a water level at the outlet of 7.61 mTAW. Results for the high added flow variant are shown in Figure 17. Notice there is a clear migration corridor forming along the domain from the fishpass entrance towards the last slot (inlet) from the vertical-slot channel. Flow patterns there are somewhat regular and velocities do not exceed 1.1 m/s. On the other hand, flow streamlines emerging from the pipe-basin system exhibit more irregular patterns and higher velocities close to the walls of the channel where velocities can reach beyond 1.5 m/s at some locations. On the other hand the results for low added flow in the fish passage shown in Figure 18 depict flow patterns similar to those presented for the high added flow case, but where velocities do not exceed 1.5 m/s. The overall efficiency of the flow within the outflow channel is improved by the modifications proposed.

5.4 Concluding remarks

The present work condenses and expands upon previous studies conducted by external parties, with a focus on the evaluation of the hydrodynamics of the added flow within the downstream reach of the fishpass. Studies performed by IMDC with geometries proposed by the designer exhibit flow features that are in contravention with the guidelines proposed in Visser *et al.* (2024), thus making the proposed designs "un-friendly" for fish migration. On the other hand, proposed improvements in the original designs studies by IMDC and later modelled by FH exhibit features that are more amenable for fish migration. In particular, by splitting the added flow in alternating pipe-basin inflows improve overall performance of the fish passage. Note that the latter improvement has a more marked effect compared to the use of guide vanes, as already mentioned earlier.

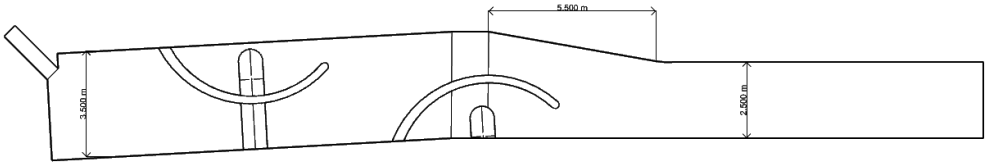

(a) Modifications to the geometry originally studied by IMDC.

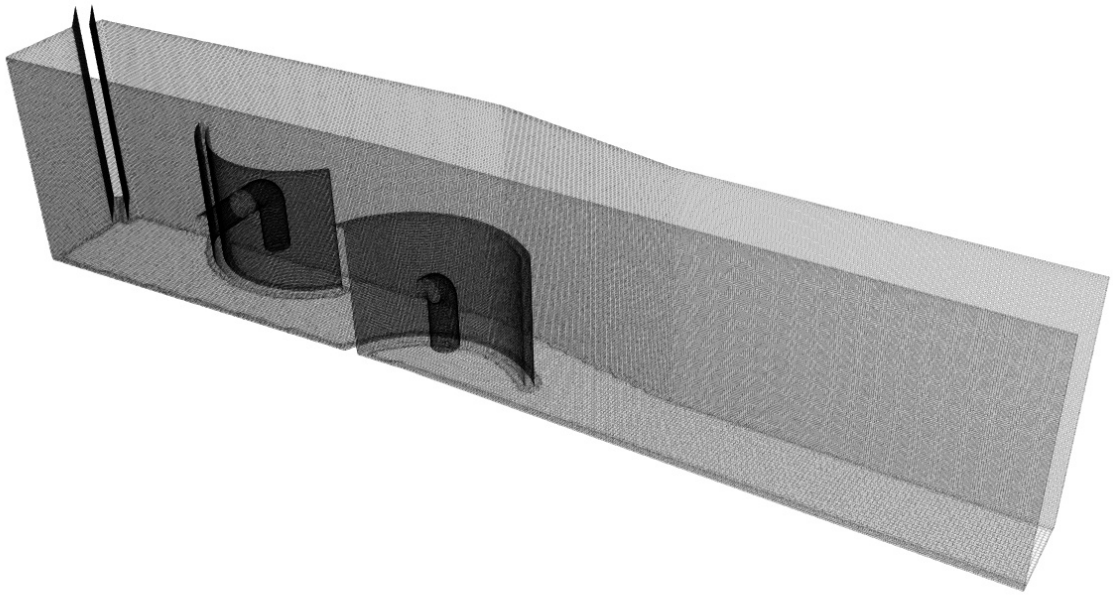

(b) Topology of the mesh.

Figure 16 – Added flow with two basins and a contraction in the fish passage entrance.

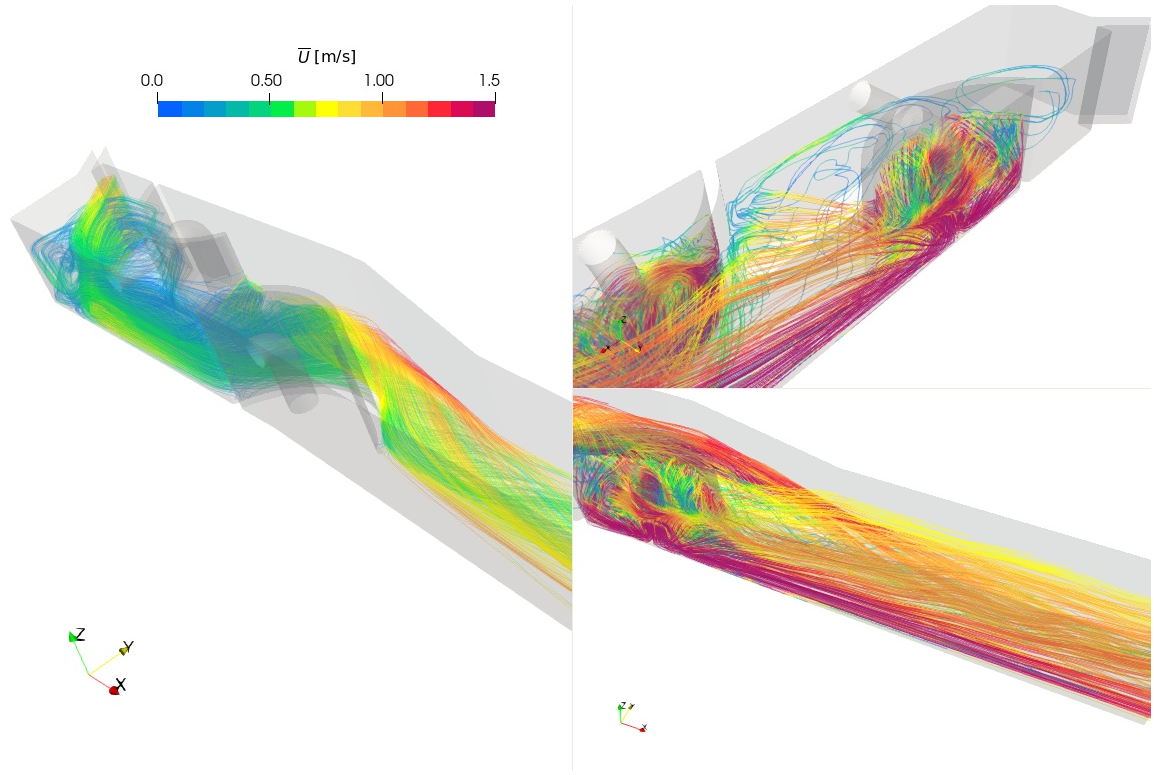

(a) Three-dimensional streamline patterns within the fish passage.

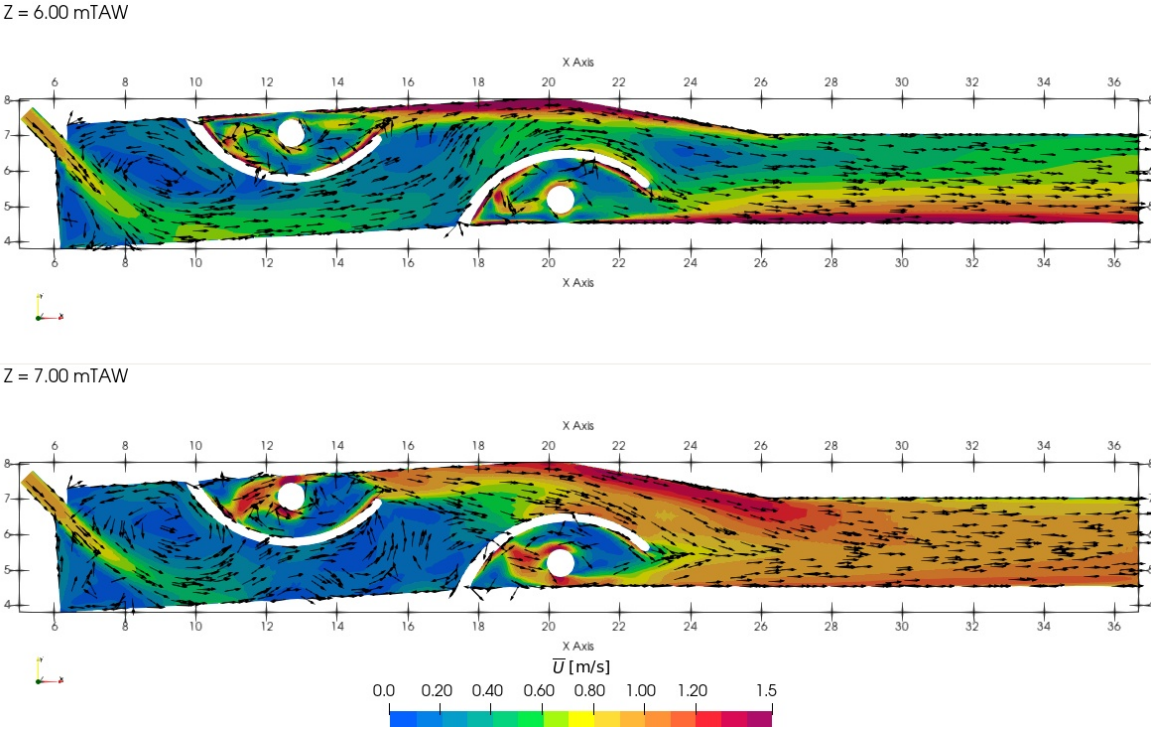

(b) Horizontal planes at different vertical location.

Figure 17 – Results for high added flow with two basins and a contraction in the fish passage entrance.

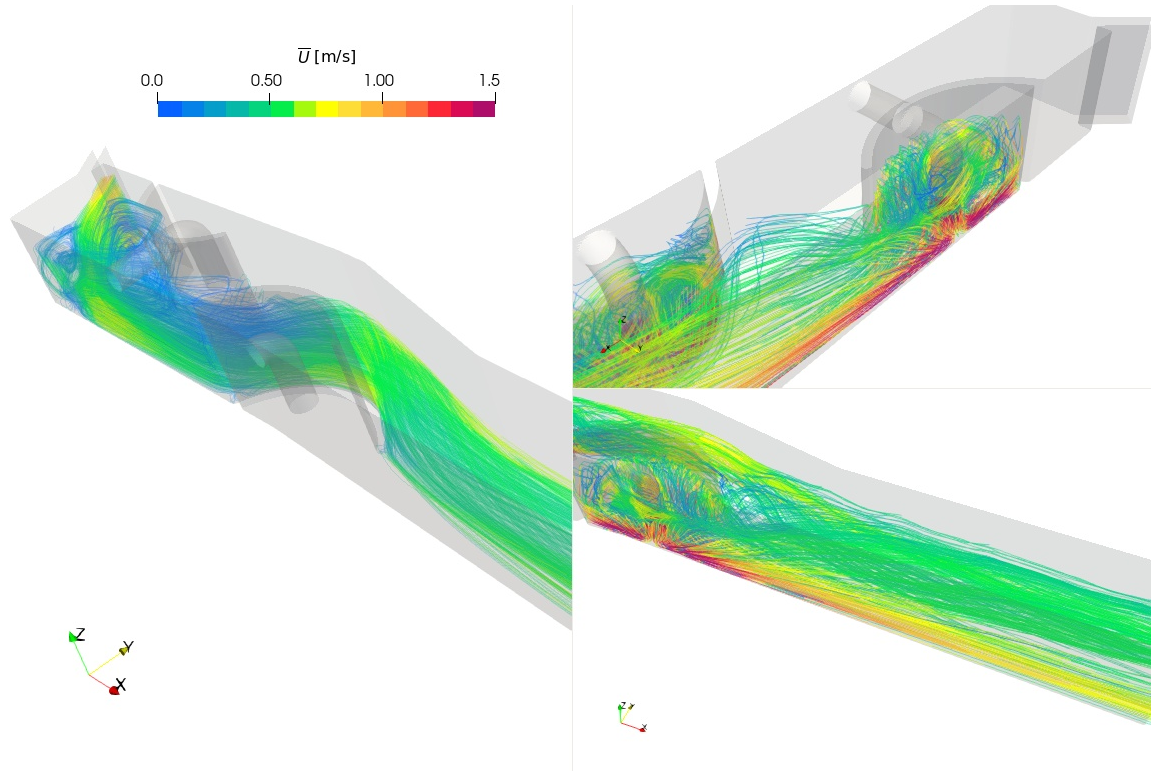

(a) Three-dimensional streamline patterns within the fish passage.

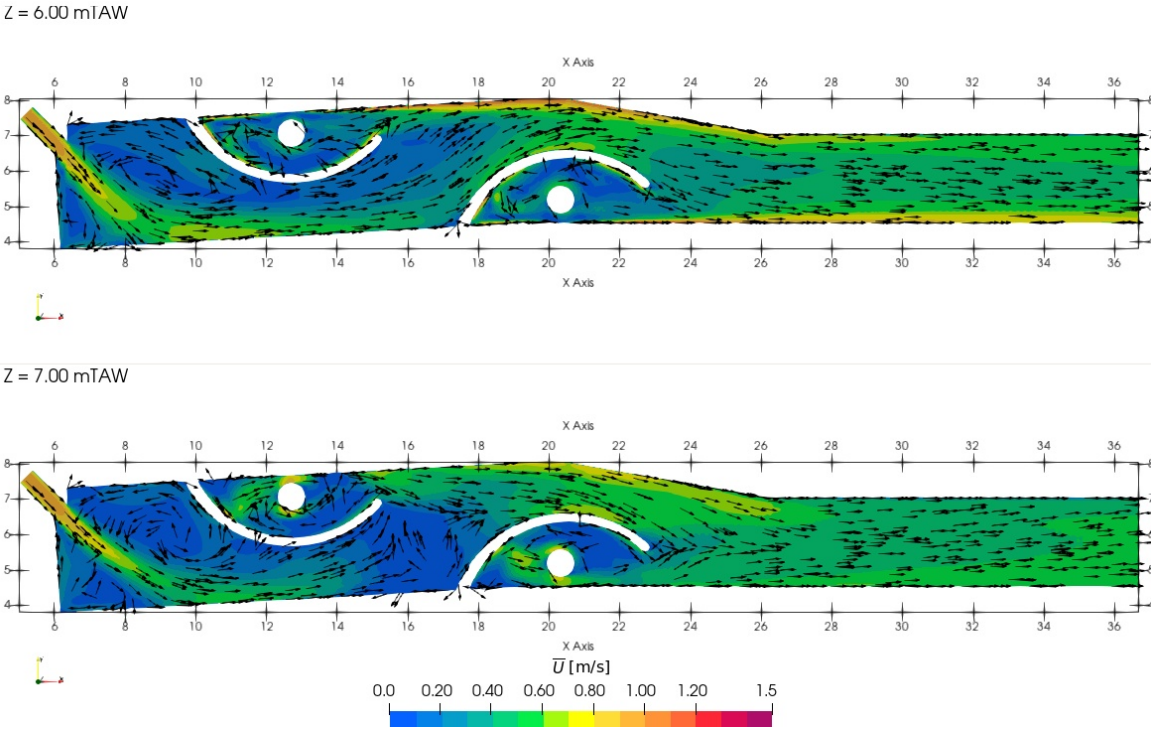

(b) Horizontal planes at different vertical location.

Figure 18 – Results for low added flow with two basins and a contraction in the fish passage entrance.

References

Badano, **N.; Breugem**, **A.; Decrop**, **B.** (2019). CFD-modellering vispassage Denderleeuw. *techreport*. IMDC

Castano, **S. L.; Hoydonck**, **W. van; Mulder**, **T. D.; Raouwens**, **P.** (2023). On the numerical resolution of hydraulic jumps: Algorithms, Boundary Conditions, and Turbulence Models. *techreport*. Flanders Hydraulics

Menter, **F.; Egorov**, **Y.** (2005). A Scale Adaptive Simulation Model using Two-Equation Models. en. ***in**: 43rd AIAA Aerospace Sciences Meeting and Exhibit*. American Institute of Aeronautics and Astronautics: Reno, Nevada. ISBN: 978-1-62410-064-2. DOI: 10.2514/6.2005−1095

Ubbink, **O.; Issa**, **R.** (1999). A method for capturing sharp fluid interfaces on arbitrary meshes. *Journal of computational physics 153 (1)*: 26–50 pp.

Visser, **K.; Buysse**, **D.; Goormans**, **T.; Viaene**, **P.; Coeck**, **J.** (2024). Vispassage op de Dender te Denderleeuw: Hydraulisch ontwerp. *Versie 3.0. WL Rapport*, 14-128-2. Waterbouwkundig Laboratorium

Visser, **K.; Buysse**, **D.; Viaene**, **P.; Goormans**, **T.; Vanderkimpen**, **P.** (2022). Vertical slot vispassage op de Schelde te Merelbeke: Hydraulisch ontwerp. *techreport*, 18-144-1. Waterbouwkundig Laboratorium

A1 Flow patterns in aerated flow: theory and numerical analysis

In addition to the results presented in previous chapters an ad-hoc analysis of the pressure fields obtained for scenario S2-A in Badano *et al.* (2019) was performed, which reveals that despite an average adverse streamwise pressure gradient being present along the dissipation bucket and in the channel downstream there is no flow detachment as a consequence. On the other hand, the simulations conducted within FH (S2-A-FH hereinafter) show separation of the flow after the bucket and a subsequent recirculation pattern, supported also by the presence of an adverse streamwise pressure and density gradients along and after the bucket. Given that the specific energy at the outflow should be the same in both simulations (at least for S2-A-FH it is), the fundamental difference between the two cases stem on how the excess kinetic energy upstream is being cancelled via head losses, more precisely:

S2-A Seems to dissipate the excess kinetic energy via an enlarged viscous boundary layer downstream from the bucket, in addition to the drowned hydraulic jump. That can be roughly observed by following the velocity iso-lines in Figure 19(a) as the core of the flow moves up and downstream towards the exit in a linear fashion.

S2-A-FH Seems to dissipate the excess kinetic energy via a bottom recirculation starting near the end of the bucket and extending downstream in the channel, in addition to the drowned hydraulic jump.

The present analysis will be conducted in two parts: (1) one where density is kept fixed in the fluid flow, and (2) another where density variations are allowed. Both discussions will contain both analytical and numerical studies which will support the hypotheses therein posed. With this, we intend to show that:

- for simulation S2-A there are two mechanisms producing local energy losses for the flow in the tailrace. One of those mechanisms is the drowned hydraulic jump produced after the jet drop, and the second mechanism is the increase of local streamline's curvature produced by the vertical widening of the channel. However, the shortened length of the surface roller after the hydraulic jump indicates over-dissipation in the simulation.
- for simulation S2-A-FH the flow streamline's curvature is further heightened by the increase of the flow's inertia downstream, as a consequence of air entrainment (aeration, bulking) produced by the drowned hydraulic jump. The unbalanced inertia manifests as an additional bottom roller which bears no direct relation to the surface roller produced by the drowned hydraulic jump, except that of the latter aerating the flow. This results in a third mechanism of energy dissipation.

Up until now, the analysis of the flow has been conducted under the assumption that density takes no part in the solution of the problem. However, as the results show for the present study, differences not only on the treatment of the inlet/outlet boundary conditions but also the approximate resolution of flow aeration plays a fundamental role in the physics being described using CFD.

A1.1 On the mechanisms producing local losses in the absence of aeration

The question that needs to be addressed is whether it's possible to have more than one flow feature (i.e. recirculations, rollers) producing local energy losses, via *internal* energy dissipation; in other words, whether a (drowned) hydraulic jump is the only possible mechanism of local energy dissipation in this case. More precisely, using one-dimensional hydraulics, the following needs to be proven:

> In the absence of bed friction, and assuming constant density, there are *at most* two separate flow features producing energy losses downstream from the weir in case S2-A.

Or more generally:

> In the presence of a channel drop, a subcritical channel flow that suffers no change in its water elevation experiences a local head loss independent of inflow and outflow Froude number.

An analysis of energy losses in a selected portion of the downstream section of the domain (as depicted by region enclosed in a box in Figure 19(a)) may be performed via 1-D hydraulics. Since the water level in the downstream level is controlled somewhere downstreams (another weir) it is safe to assume that, in the absence of aeration, the water level remains roughly constant along the section. This is confirmed by the results obtained for the S2-A simulation shown in Figure 19(a). A first idealization of the flow may be made assuming (a) there's no *drowned* hydraulic jump, that is, the flow is subcritical upstream as shown in Figure 19, (b) water level does not vary along the channel, (c) there is no confluence at the toe of the slope[5], and (d) the channel is wide. Disregarding wall-friction losses, and Coriolis coefficients, a naive interpretation of the energy balance will show the following contradiction:

$$E_1 = E_3, \tag{4}$$

$$\Delta Z + y_1 + \frac{(V_1)^2}{2g} = y_3 + \frac{(V_3)^2}{2g}, \tag{5}$$

$$= (\Delta Z + y_1) + \frac{(V_3)^2}{2g}, \tag{6}$$

$$\frac{(V_1)^2}{2g} = \frac{(V_3)^2}{2g} \text{ Contradiction!} \tag{7}$$

Clearly, due to mass conservation, the velocity at the inflow must be larger than at the outflow; hence the correct interpretation of the energy in the system is the following:

$$\frac{(V_1)^2}{2g} > \frac{(V_3)^2}{2g} \Rightarrow \tag{8}$$

$$E_1 = E_3 + \Delta h, \tag{9}$$

where Δh is a local energy loss, equal to the excess kinetic energy between the end sections. The energy loss in this case manifests as an adverse pressure gradient, or flow deceleration, which imply local curvature and/or distancing between the flow streamlines.

Unfortunately, it is not possible to obtain an expression for the energy losses since it would require that the pressure distributions at the inlet and outlet of the channel would be different from hydrostatic if the forces against the step are also included in the analysis which, for this scenario, is not realistic to assume. In other words, for the present case, with a rigid-lid, a non-hydrostatic distribution of pressures around the step is necessary in order to drive the flow. A local, adverse, pressure gradient on the step can only be locally balanced by a local drop in water level, a local acceleration, a change in fluid density, or an external force such as the weight of the fluid in case of a sloped channel.

As a first step, one may assume that the horizontal hydrostatic pressure forces acting on the drop are negligible relative to the momentum flux at the inlet and outlet, i. e. The drop is small. One may also, alternatively, assume that the horizontal forces acting against the step are greatly reduced due to the drop in density produced by the bulking within the weir's bucket hence they could safely be ignored. A momentum balance between the two sections with unit discharge q, assuming the forces on the step are small compared to the momentum fluxes, may help finding an expression for Δh, as follows:

[5] This assumption, as it will be shown later, is of no consequence for the present proof.

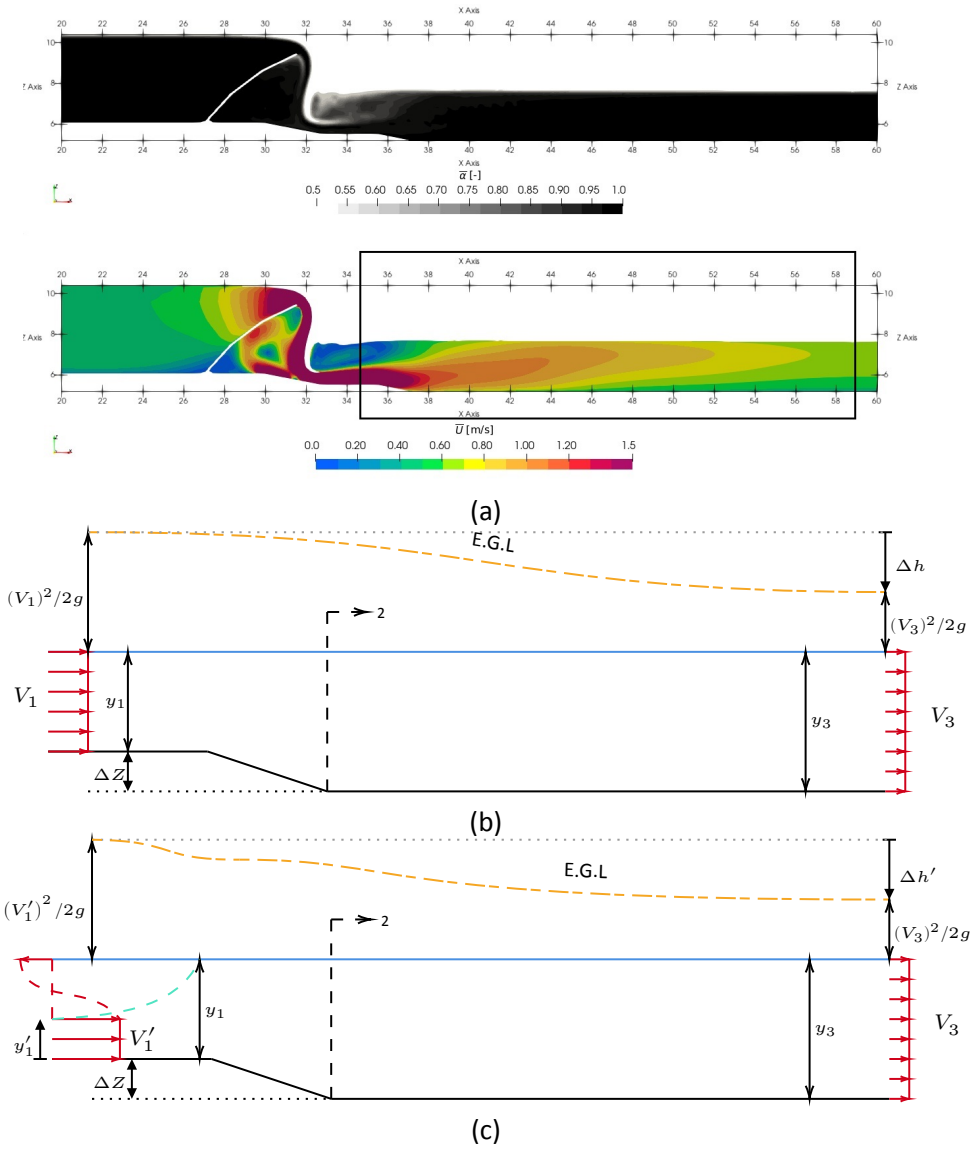

Figure 19 – Analysis of section of the weir complex for scenario S2-A. (a) Velocity field and air phase-fraction presented in Badano *et al.* (2019), where the section of interest is indicated by the black box; (b) first idealization of the flow, ignoring the drowned hydraulic jump, (c) refined idealization considering the drowned hydraulic jump.

$$\sum F_x = \rho q\,(V_3 - V_1) \Rightarrow$$

$$\frac{g}{2}y_1^2 - \frac{g}{2}(y_1 + \Delta Z)^2 = q\,(V_3 - V_1)\,,$$

$$(\Delta Z)y_1 + \frac{1}{2}(\Delta Z)^2 = \frac{q^2}{g}\left(\frac{1}{y_1} - \frac{1}{y_3}\right),$$

and by combining the previous expression with Equation 9 one finally obtains the following:

$$(\Delta Z)y_1 + \frac{1}{2}(\Delta Z)^2 = (2\Delta h)\left(\frac{y_1 y_3}{y_1 + y_3}\right), \tag{10}$$

$$4\frac{\Delta h}{\Delta Z} = \frac{(y_1 + y_3)(2y_1 + \Delta Z)}{y_1 y_3}, \tag{11}$$

$$\frac{\Delta h}{\Delta Z} = \frac{(y_1 + y_3)^2}{4y_1 y_3}. \tag{12}$$

Notice the striking similarity of Equation 12 with the theoretical expression of energy loss in classical hydraulic jumps. Additionally, this expression is exactly equal to that for a bump in a straight channel. Clearly, as the ratio y_3/y_1 approaches one then

$$\frac{\Delta h}{\Delta Z} \to 1.$$

Notice that the previous expression suggests that the local losses due to the step are *at least* as large as the step's height[6] for limiting cases (Very low Froude Number or very small steps), indicating that an additional energy loss mechanism as the ratio $y_3/y_1 > 1.0$ thus proving our initial "theorem". This idealization, however, doesn't offer a clear indication of how the energy loss produced by this mechanism (flow separation, adverse pressure gradient) can be estimated or when it may occur.

Given the challenges posed by the previous archetype, one may propose an idealization resembling more the dynamics of the flow seen in scenario S2-A; that is, a flow including a drowned hydraulic jump and a channel drop, as shown in Figure 19(c). This archetype allows for a direct description of the energy losses using energy and momentum arguments. In other words, there is an additional mechanisms dissipating energy in this idealization (possibly 3), the new one being the surface roller produced by the jump. Following the same approach as before and the notation shown in Figure 19, the energy balance between the inlet and outlet sections is:

$$\frac{(V_1')^2}{2g} = \frac{(V_3)^2}{2g} + \Delta h', \tag{13}$$

from which one can derive the following inequality:

$$\frac{(V_1')^2}{2g} \geq \frac{(V_1)^2}{2g} > \frac{(V_3)^2}{2g} \Rightarrow \tag{14}$$

$$\Delta h' \geq \Delta h, \tag{15}$$

showing that indeed there must be an additional mechanism of energy loss (besides the step, and perhaps the flow separation). Obtaining an expression for the energy loss requires the assumption of a small step and additional assumptions about pressure distributions, which may clearly under-predicts the effect of flow separation or adverse pressure gradients in the flow.

The validity of the present analysis is proven with 2D numerical representations of the two idealizations just explained, as shown in Figure 20. The 2D simulations are made run with a canonical discharge of 1.58 m^2/s (corresponding to half the discharge of the channel divided by the width of one weir for S2-A), and the geometry of the bottom is similar to the profile of the bucket and tailrace in S2-A and an upper rigid lid in order to enforce the assumptions just discussed. The only difference between the two simulations is the inflow: one where a bottom opening of 50 cm is used, and other where the discharge is allowed to pass across the whole wetted section.

Note on the lower plate in Figure 20 that the flows undergoes local acceleration near the upper tip of the slope and then gradually decelerates towards the toe of the slope, indicating an adverse pressure gradient in the flow. On the other hand, the upper plate clearly shows the recirculation region overwhelming all other energy-loss mechanisms present in the flow.

The present analysis and numerical results are also valid for the case where more than one upstream channel *merges* with the channel downstream at the toe of the slope (section 2 in Figure 19), since the confluence of the three tributaries (2 weirs and the fish passage) represents a *hydraulic control* where energy must be kept equal. More simply expressed, in the absence of bottom friction:

$$E_{\text{upstream}} = E_2 + \Delta h'',$$
$$E_2 = E_3,$$

where E_{upstream} refers to the energy at each of the tributaries.

[6] Notice that this solution corresponds to the energy loss after a sill in a straight channel.

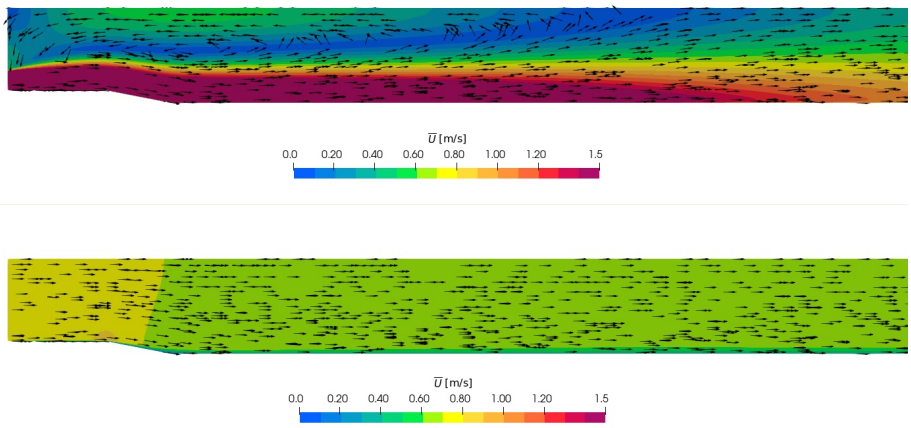

Figure 20 – Results obtained for the two idealizations studied. No bottom roller is seen in either case.

A1.2 On the mechanisms producing local losses in aerated flows

On previous discussions it has been shown that there are two mechanisms producing energy losses in the tail race, not related at all with bottom friction and independent of density variations. When observing the results from simulation S2-A-FH (shown in Figure 21(a)), one concludes that density variations in the region comprising the drowned hydraulic jump and surface roller are non-negligible and that such must be considered in the present desktop calculations. Furthermore, density variations due to *bulking* may increase somewhat the water level locally close to section 1. This implies there must be an additional mechanism producing an energy loss corresponding to such increase. In general, what it will be shown here is that:

> In the absence of bed friction and considering aeration in the incoming flow there is an additional, separate, flow feature producing energy losses downstream from the weir in case S2-A-FH in addition to the two already discussed in previous sections for S2-A.

For this proof a different idealization of the flow is needed, as shown in Figure 21(b). Note there that despite there being a local increase in water height at the drowned hydraulic jump, this increase can be conservatively ignored by assuming the vertical pressure distribution at this region to be linear and density variations to be uniform across the height. This is done to ease the discussion, and should bear no implication in the analysis that follows.

Including integral-averaged density variations on classical hydraulic desktop calculations can prove challenging, particularly if one expects to draw general conclusions out of the analysis being performed. Here density variations will be considered heuristically just by performing an spatio-temporal averaging (denoted by $\langle\overline{(\cdot)}\rangle$) the water phase-fraction at the region encompassing the drowned hydraulic jump in Figure 21(a), obtaining $\langle\overline{\alpha}\rangle = 0.65$ (on the other hand, the water fraction in the same region for simulation S2-A is about $\langle\overline{\alpha}\rangle = 0.86$).

Clearly, under similar inflow and outflow conditions, the sudden increase in density at the tailrace after the bucket acts somewhat as a barrier to the incoming flow. This can be readily seen by comparing the specific force at section 1 from the un-aerated and the aerated case:

$$\frac{\rho_{\text{water}}g}{2}y_1^2 + \rho_{\text{water}}qV_1' > \frac{\rho_{\text{mix}}g}{2}y_1^2 + \rho_{\text{mix}}qV_1', \tag{16}$$

where clearly the momentum in the aerated case is in average $\rho_{\text{mix}}/\rho_{\text{water}} = 0.65$ times that of the un-aerated case. This implies that there must be an additional internal force relative to the two scenarios that must overcome the difference in densities and balance the momentum at the outlet, that is, in the limit of a small step:

$$\sum F_x = \rho q \left(V_3' - V_1'\right) \Rightarrow$$
$$\frac{\rho_{\text{mix}} g}{2} y_1^2 + \rho_{\text{mix}} Q V_1' + F = \frac{\rho_{\text{water}} g}{2} (y_1 + \Delta Z)^2 + \rho_{\text{water}} Q V_3', \tag{17}$$

where F is the aforementioned force, and V_3' is the mean velocity at section 3 which may (or may not) be different to that of previous idealizations. The location of this force can be assumed to be in the region where the fluid flow is fully de-gassed, which is more or less at section 2 (see Figure 21(b)) corresponding roughly to the region where the horizontal gradient of α seems the greatest.

Note that in previous sections it was well established that there were 2 mechanisms in which local losses occur. Both mechanisms produce an adverse pressure gradient, and here both are affected by aeration. On one hand, the degree of submergence increases somewhat at a drowned hydraulic jump and, on the other hand, the streamlines pouring down the bucket eject upwards once they arrive to section 2 due to the sudden change in inertia produced by the de-gassing of the water column, inducing a bottom recirculation. This separated flow produces additional energy losses along sections 2 and 3, which imply that for the present idealization the recirculation acts as a third mechanism of energy dissipation that is infinitely long. This contradiction is overcome by assuming a somewhat higher water height at section 2 in the idealization, equal to the head loss produced by the bottom recirculation[7]. Note also that this *bubble plume* is not driven upward by buoyancy only; rather, a heavier body of water downstream of the plume acts as a sort of partial obstacle to an incoming flow with reduced density.

Results of numerical simulations following the aforementioned idealization are presented in Figure 22(a), as a support for the aforementioned analysis. This simulation differs from the previous ones in two respects: (1) the free-surface is allowed to vary at the inlet, and (2) the inflow is assumed *aerated*, that is, the incoming mass flux considers $\rho = 0.65\rho_{\text{water}}$ in accordance to what was seen in simulation S2-A-FH. Note, in fact, that the lack of aeration in free-surface flow leads to no bottom roller, as shown in Figure 22(b) and in previous discussions. Note also that the bottom roller is indeed present in situations where density gradients are large. Additionally to that, observe that the surface roller produced by the hydraulic jump is weakened opposed to what was obtained in Figure 20 but in accordance to what is seen in Figure 21(a). Finally, water elevation between sections 1 and 2 increases somewhat compared to the water elevation in section 3 following the increased losses produced by the bottom roller.

A1.3 Concluding Remarks

This chapter discusses the physics behind the discrepancies seen between the studies conducted by IMDC (Badano *et al.*, 2019) and the verifications performed by FH, under the assumption that the results obtained by both parties reached stationarity. Given the high computational demand of the simulations involved in the present study, verifications on stationarity of the solution was only performed for the studies conducted here.

Briefly speaking, the simulations conducted by IMDC present lower degrees of aeration and bulking in the region within the buckets downstream from the weirs, compared to the simulations conducted here. Increased aeration and bulking of the jet flow below the roller of a hydraulic jump produced a bottom roller downstream of the bucket, which is explained by the adverse change in inertia between the bodies of water upstream and downstream from the bucket. It is discarded, as per the analysis just presented in this chapter, that the origin of the bottom roller is caused by over-dissipative features produced either by the turbulence model or spurious artifacts produced by incorrect meshing or use of interpolation schemes. In other words, the existence of the bottom roller may be explained as one of the three possible mechanisms of energy loss that may exist for this problem.

[7] As mentined earlier, this is not done in order to keep the discussion as simple as possible.

On the other hand, the aforementioned roller is not present in the simulations conducted by IMDC most likely because air entrainment and bulking are *under-resolved*[8] in their case. The jet impinging the tailrace from the weirs had velocities that exceed 3.5 m/s, so one expects high degree of air entrainment and turbulence produced both the subsequent surface roller and the impingement itself. Nevertheless under the assumption of little-to-no aeration the physics shown in S2-A are *plausible*, and respond to such assumption. Their simulations, however, exhibit some over-dissipative features specially in the resolution of the surface roller consequence of the drowned hydraulic jump in the weirs' stilling basin.

The length of the surface roller in simulations S2-A seem diminished when compared to the results obtained in Figure 19(b). Note that in the absence of flow bulking the length of the surface roller can be approximated as

$$L_r = 6(y_2 - y_1') \approx 11.40 \text{ m},$$

which roughly corresponds to what is being seen in Figure 19(b) (approx. 12 m). On the other hand, the surface roller depicted in Figure 19(a) is about 4 m long, somewhat shorter to the roller obtained in S2-A-FH (6 m long). In the presence of flow bulking in the water jet upstream from the roller, the degree of aeration ($\alpha < 1$) *modulates* the length of the surface and the subsequent bottom rollers, as shown in Figure 21(a).

A1.3.1 Future research

A final resolution of the present dichotomy may require either in-situ measurements or, in the least, physical scale model tests. The problem with both options is, ironically, *aeration*: measuring velocities in bubbly flows is quite complex, and producing bubbly flows at laboratory scales is also challenging. Also, the scaling of bubbly flows in laboratory scale is complex and, many times, not possible.

[8] By under-resolved we mean compared to FH simulations.

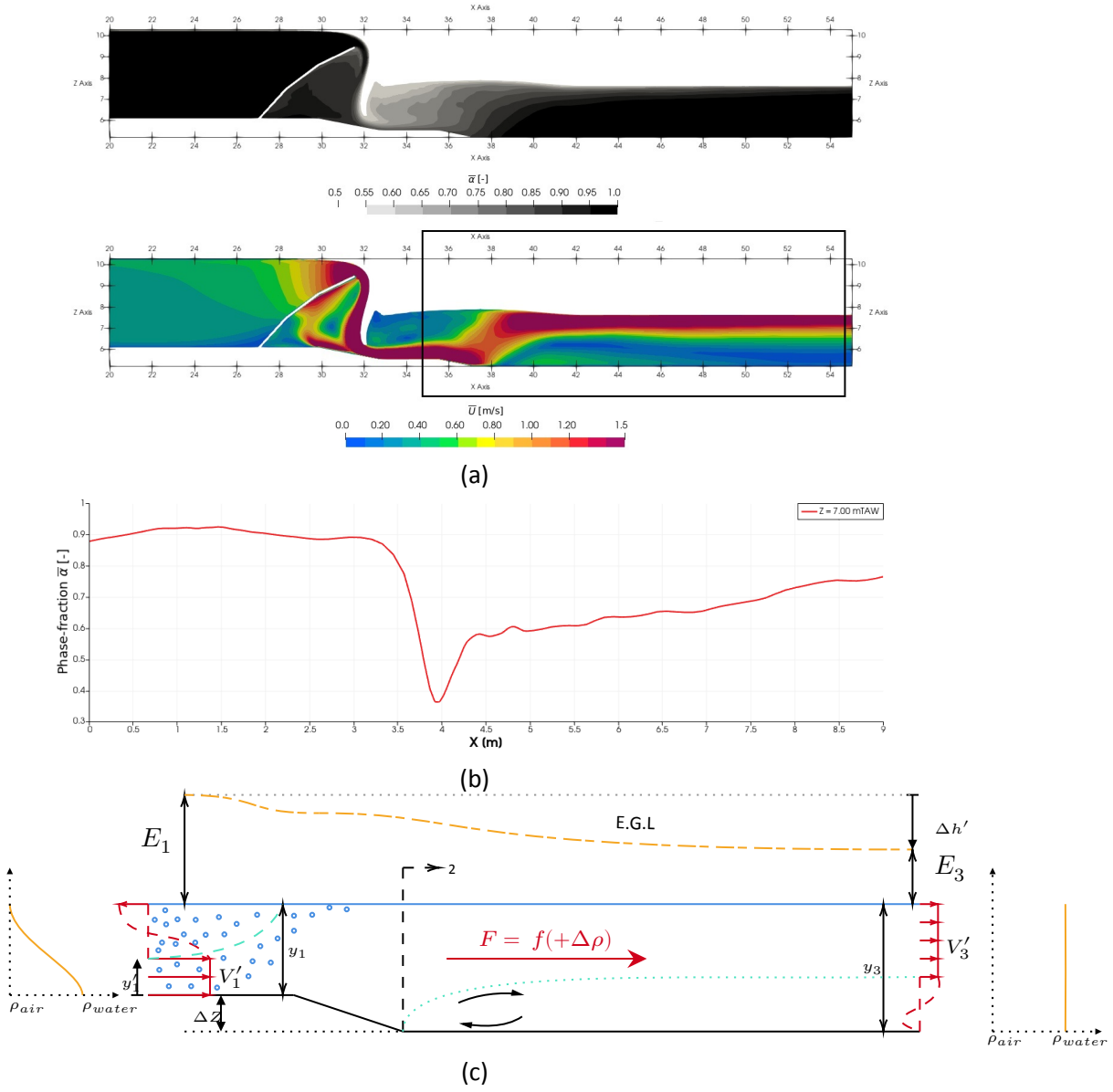

Figure 21 – Analysis of section of the weir complex for scenario S2-A-FH. (a) Velocity field and air phase-fraction obtained in the present study, where the section of interest is indicated by the black box; (b) longitudinal space-time averaged profile of the water-phase fraction within the bucket at height 7.00 mTAW; and (c) idealization of the flow assuming changes of density due to aeration.

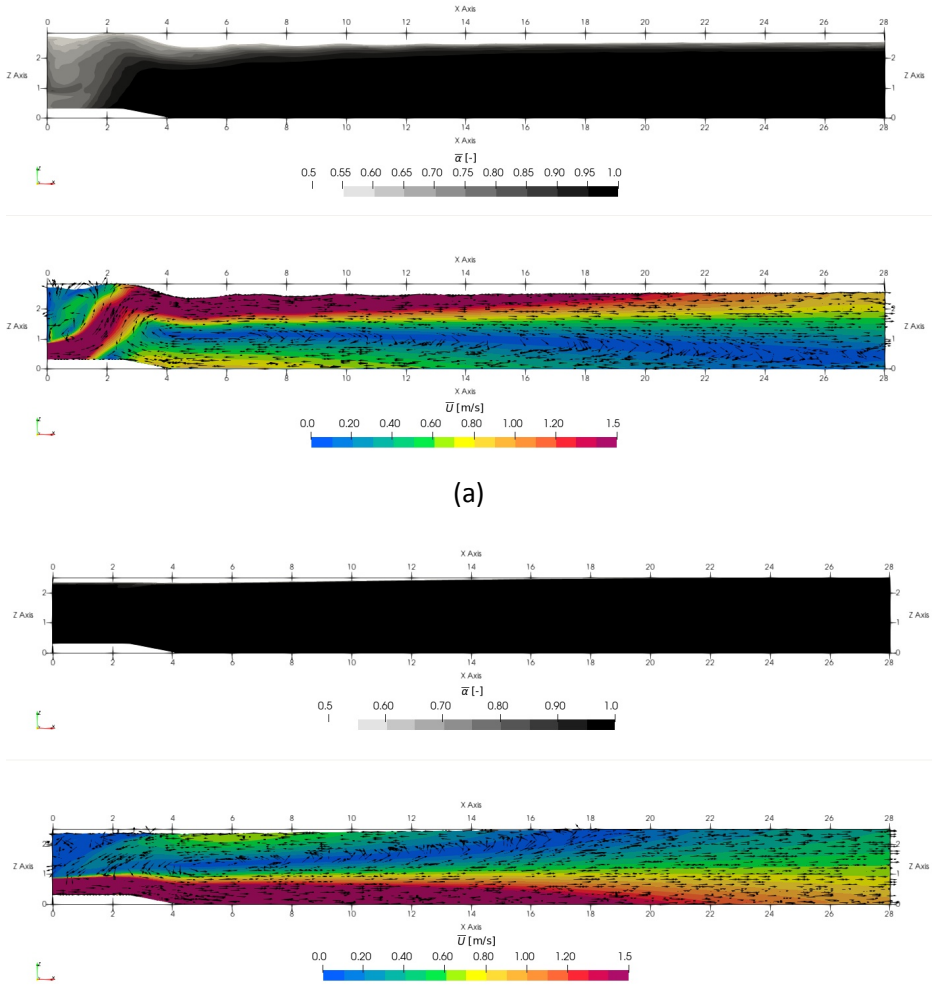

Figure 22 – VoF Results obtained for the idealization studied: (a) considering aeration and density variations at section 1, and (b) ignoring aeration. Note the shear region of the roller upstream occurs where the iso-contours of α are the closest for the aerated case.

A2 Post-procesing of simulations conducted by FH

A2.1 Modelling of the attraction flow in the tailbay

Within the present project several cross-sections from the simulations conducted by FH were requested for the analysis of the flow; the location of these sections in the domain are shown in Figure 23 and the sections themselves are shown below. It was preferred to place all of the section in an appendix in order to avoid cluttering the report. Note that some of these sections were already shown in the report.

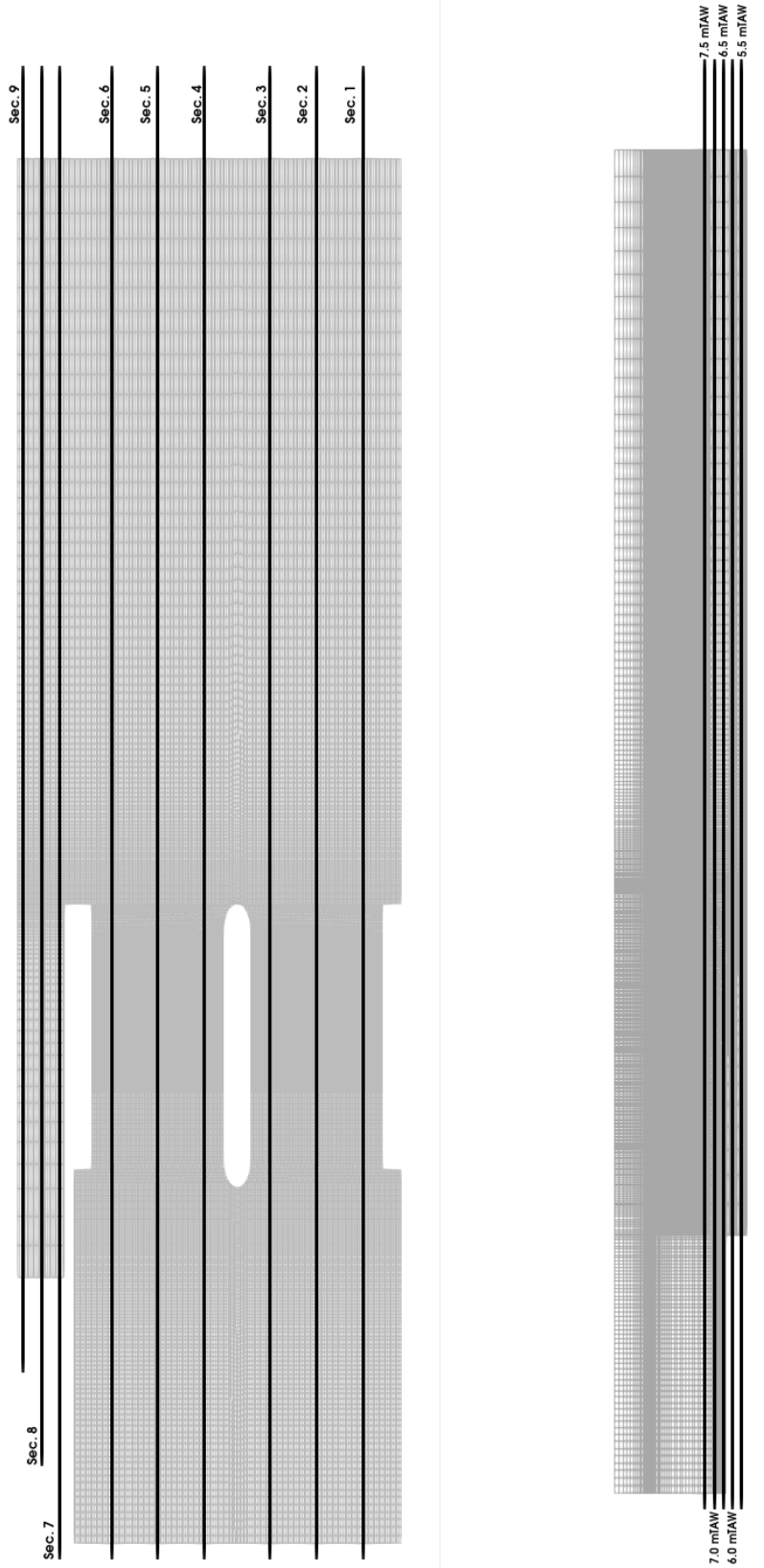

Figure 23 – Horizontal and vertical cross sections requested within the frame of the present project.

A2.1.1 BASELINE Case

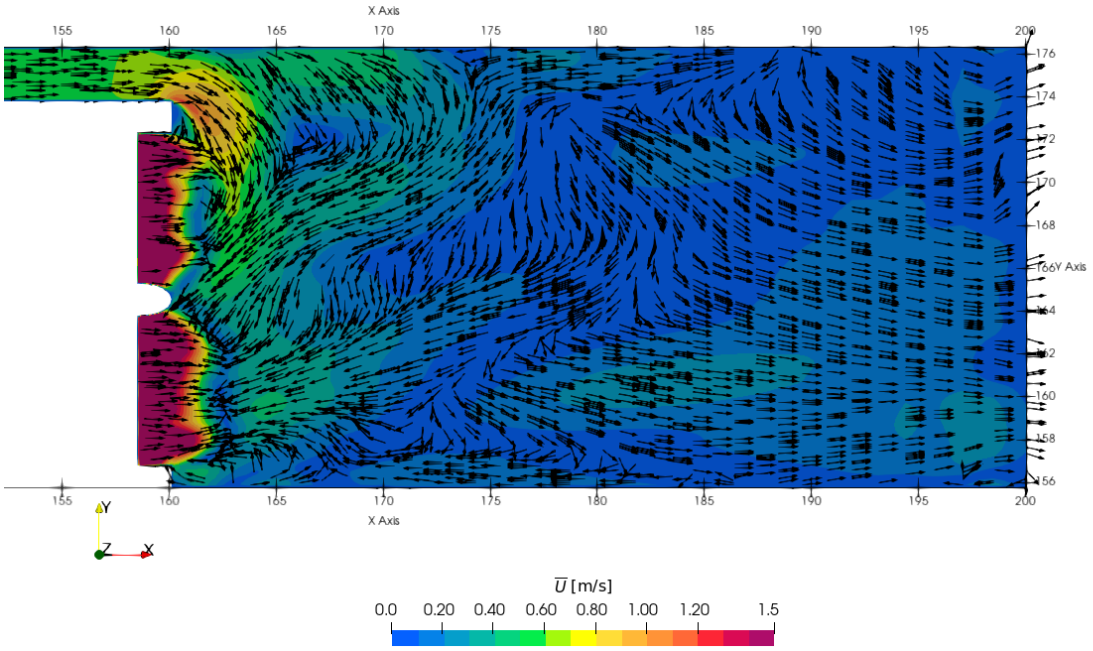

Figure 24 – Horizontal plane at Z = 5.5 mTAW.

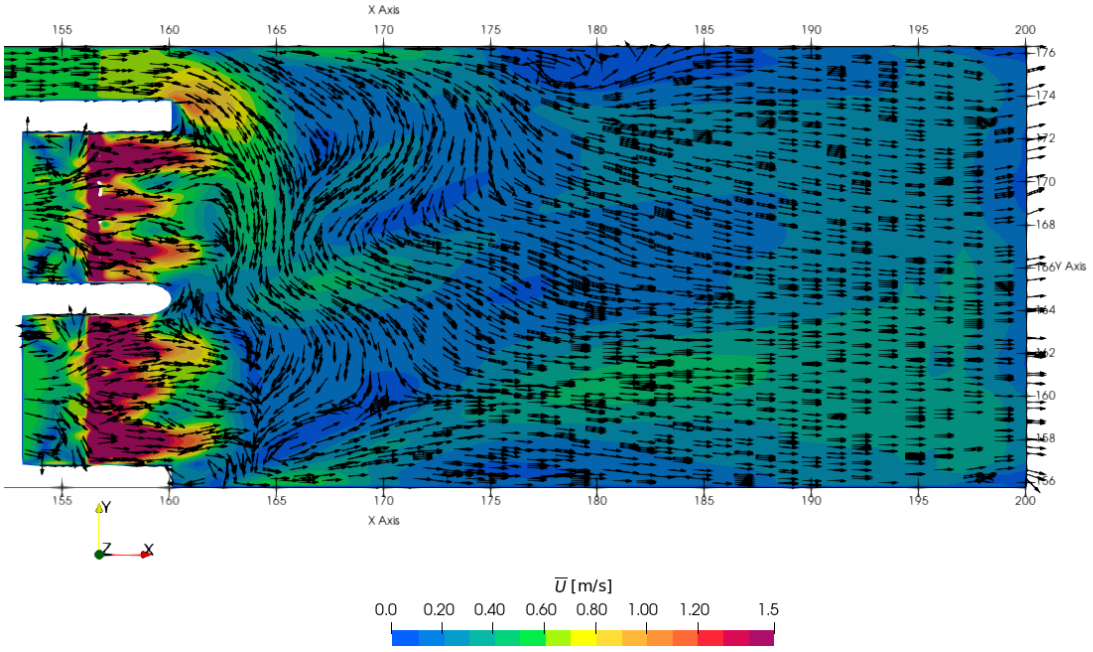

Figure 25 – Horizontal plane at Z = 6.0 mTAW.

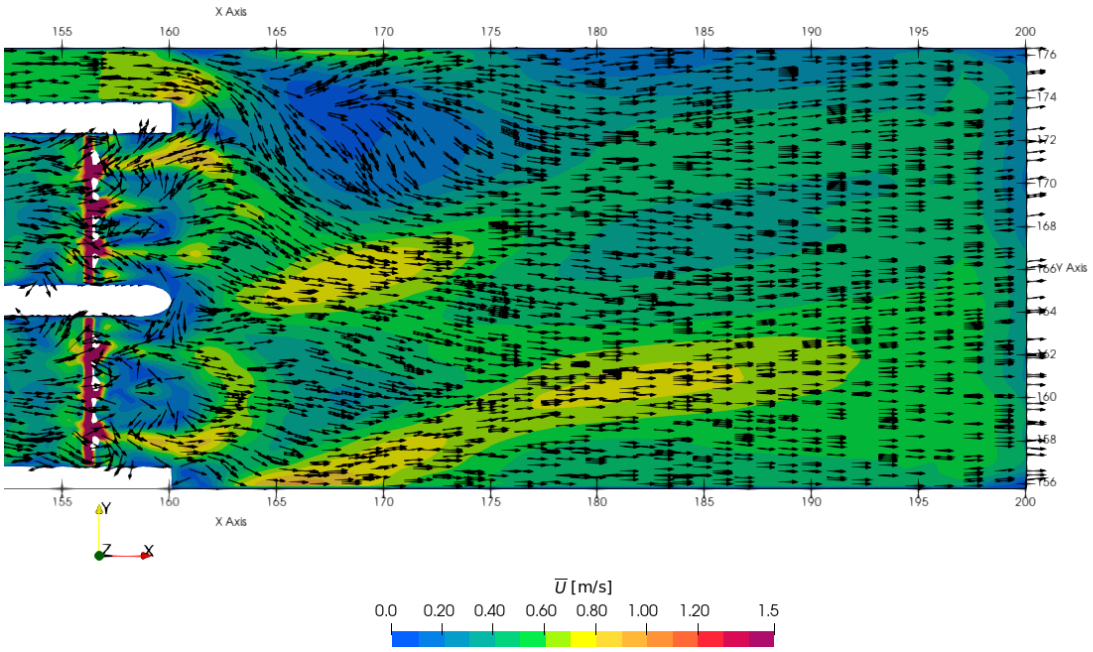

Figure 26 – Horizontal plane at Z = 6.5 mTAW.

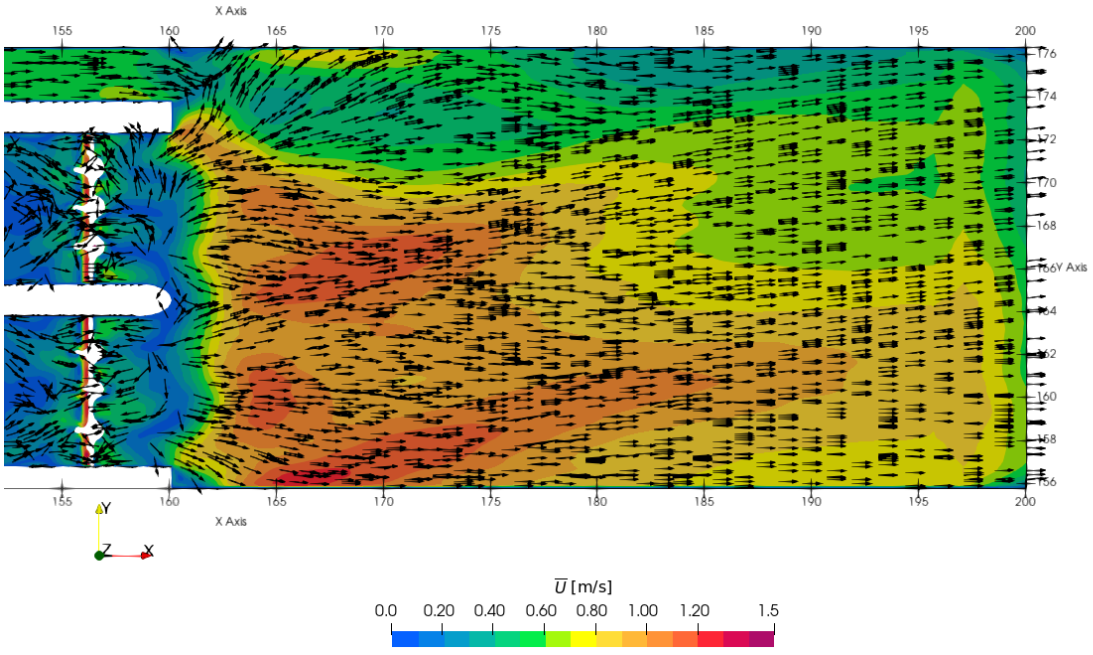

Figure 27 – Horizontal plane at Z = 7.0 mTAW.

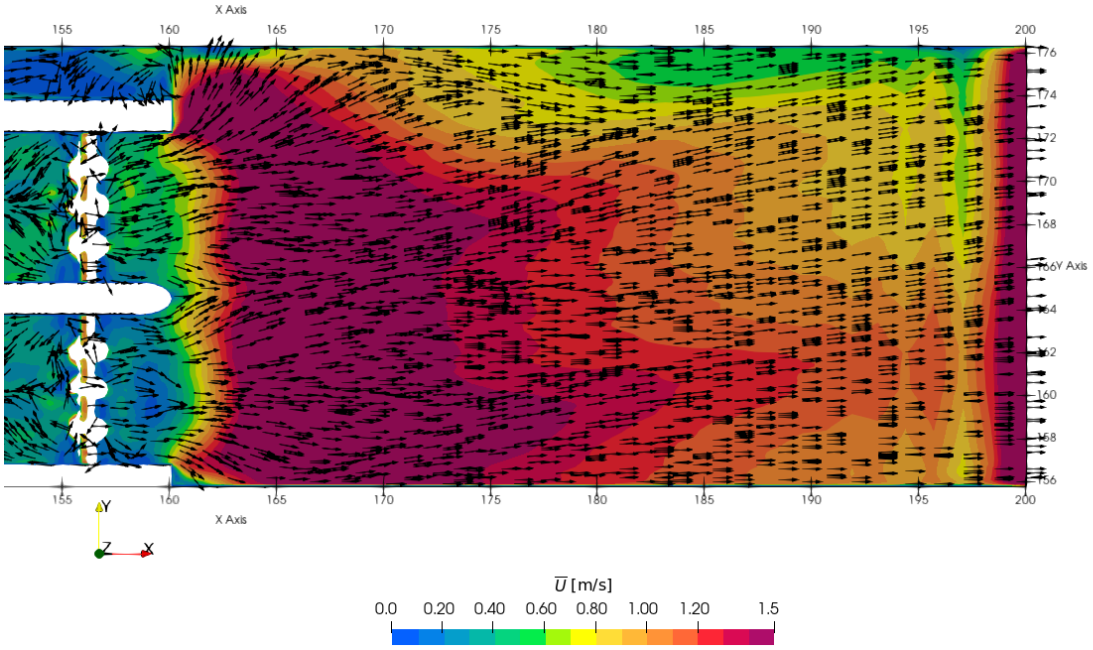

Figure 28 – Horizontal plane at Z = 7.5 mTAW.

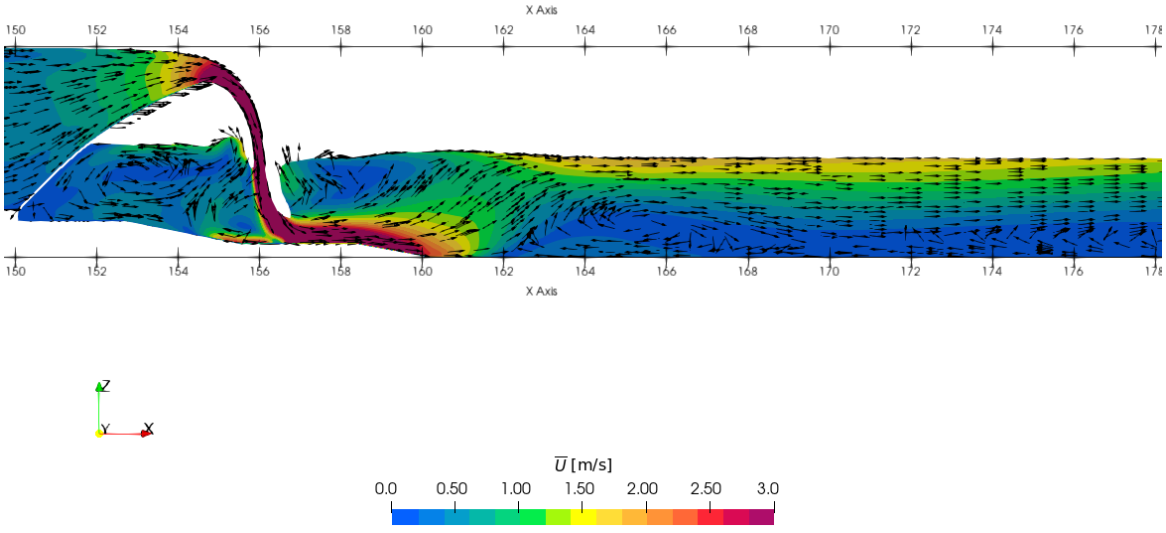

Figure 29 – Vertical Plane at Section 1.

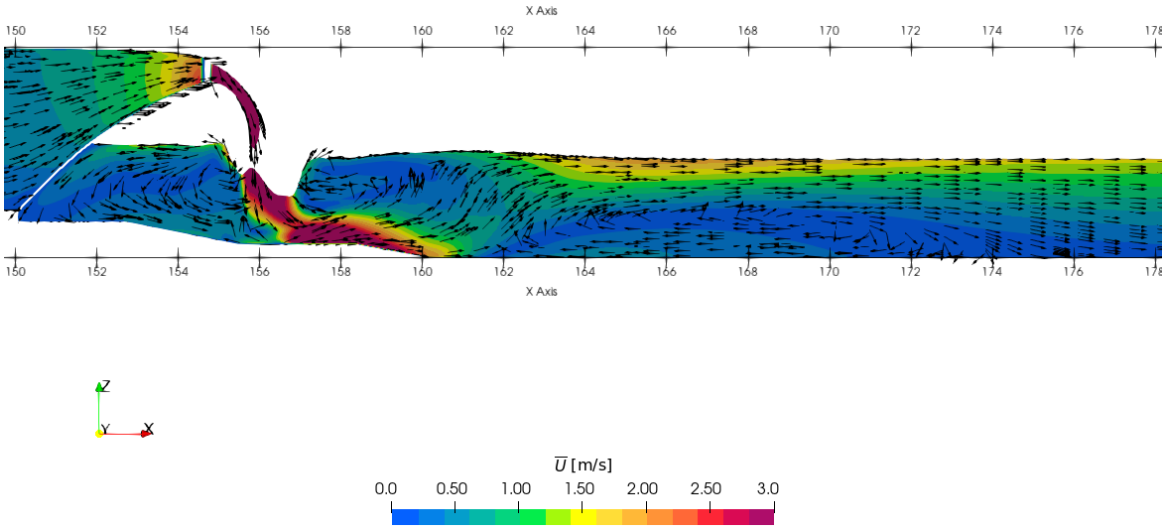

Figure 30 – Vertical Plane at Section 2.

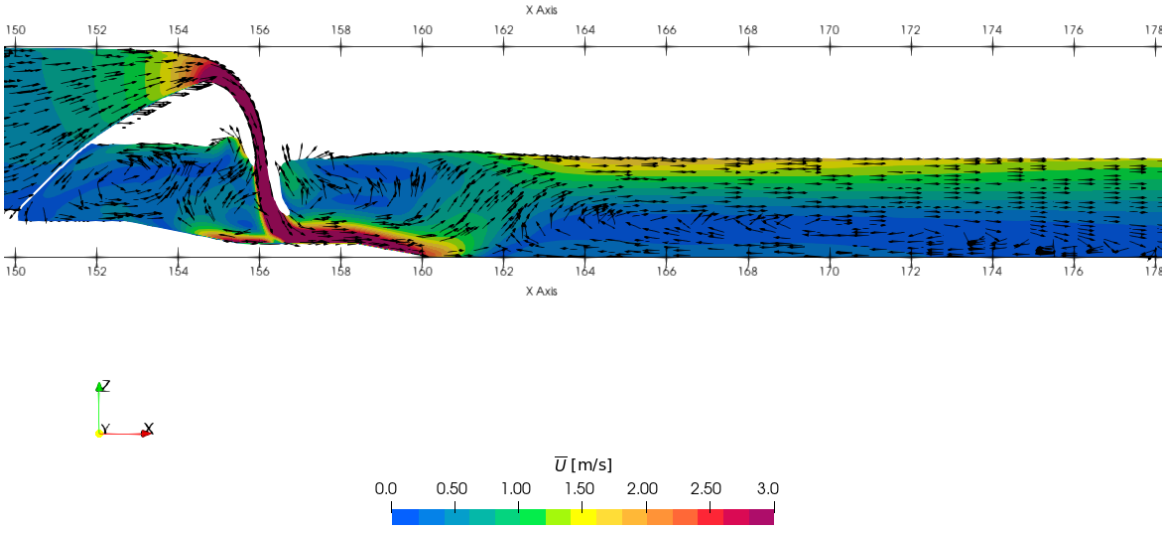

Figure 31 – Vertical Plane at Section 3.

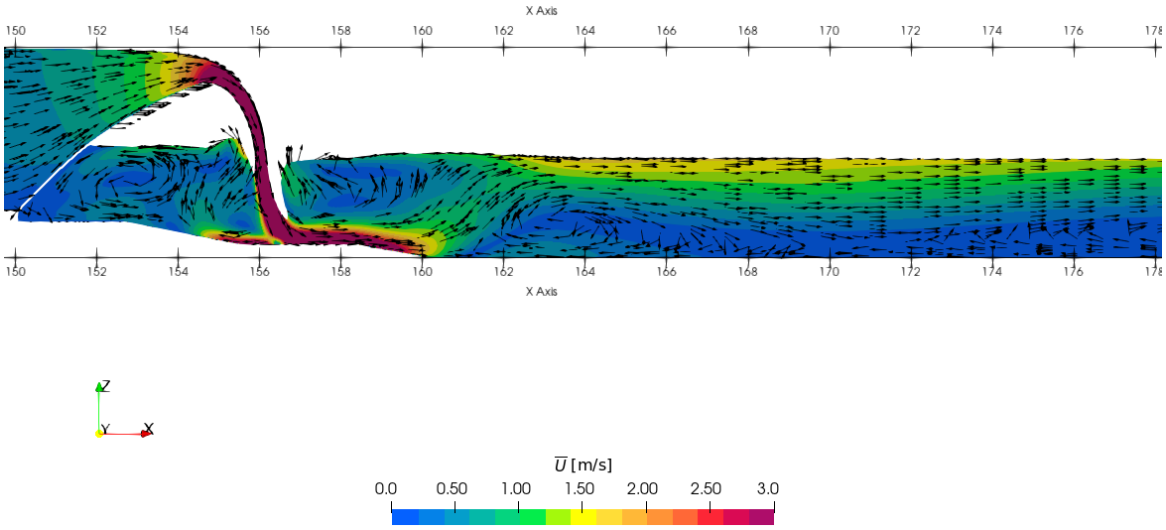

Figure 32 – Vertical Plane at Section 4.

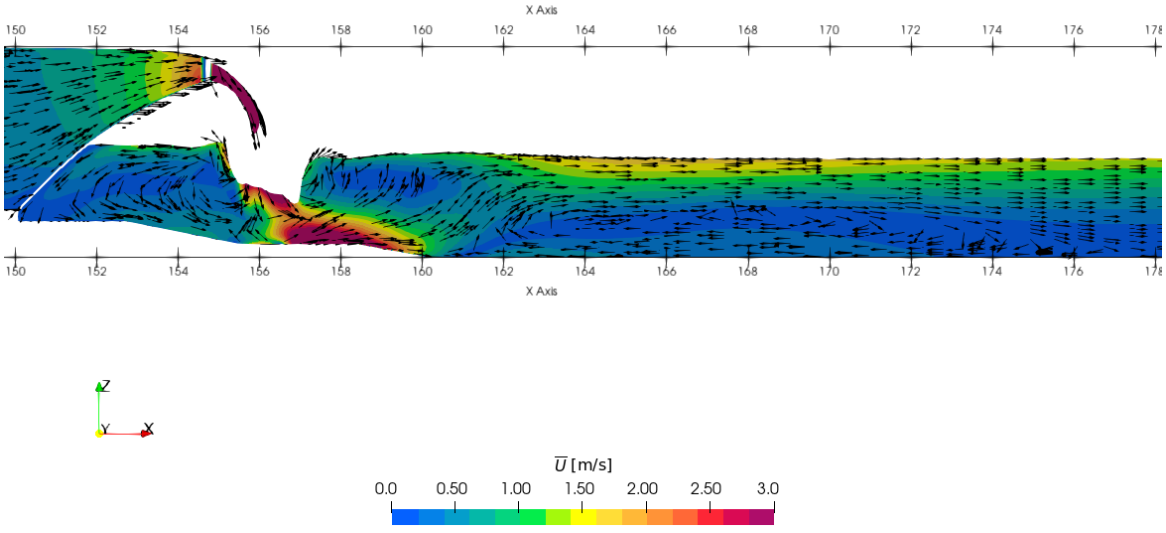

Figure 33 – Vertical Plane at Section 5.

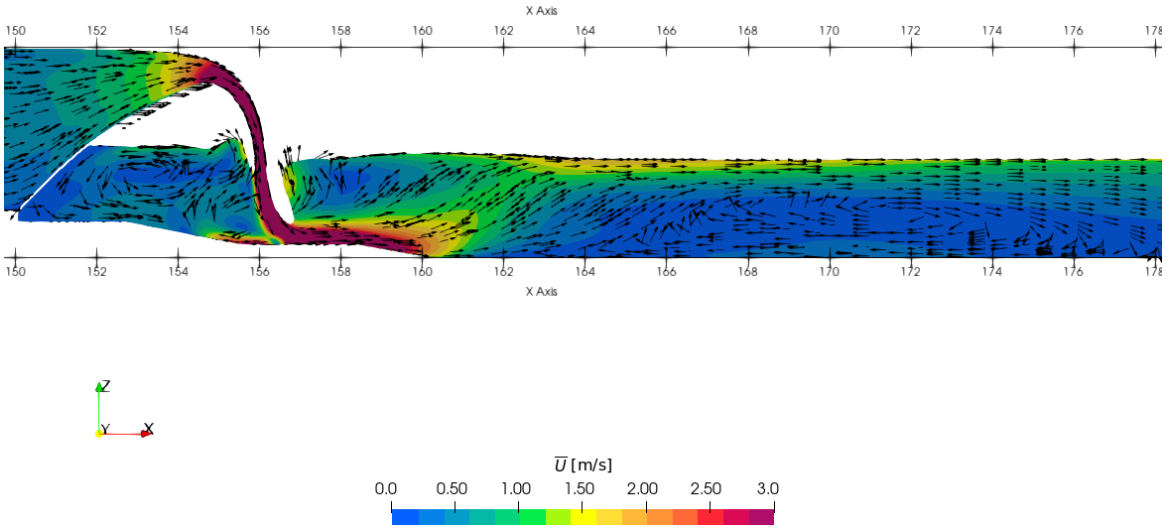

Figure 34 – Vertical Plane at Section 6.

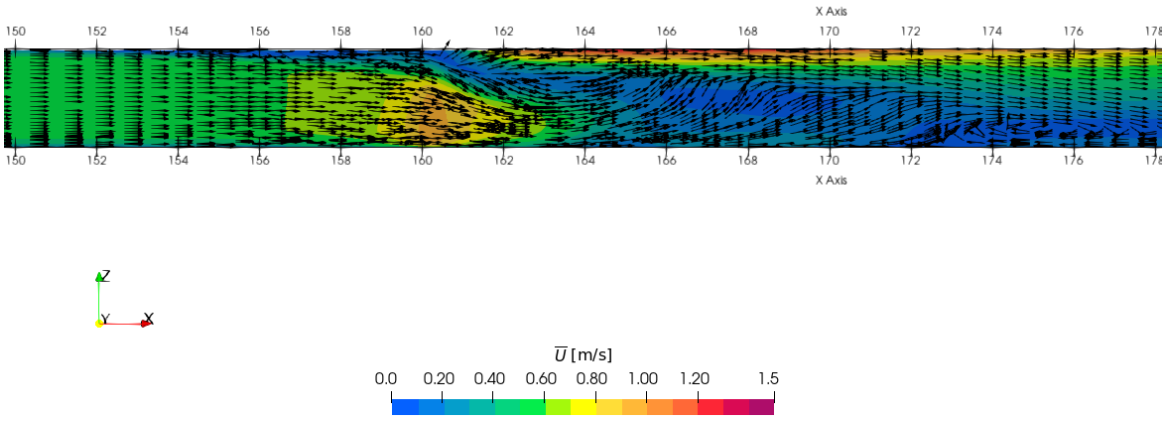

Figure 35 – Vertical Plane at Section 7.

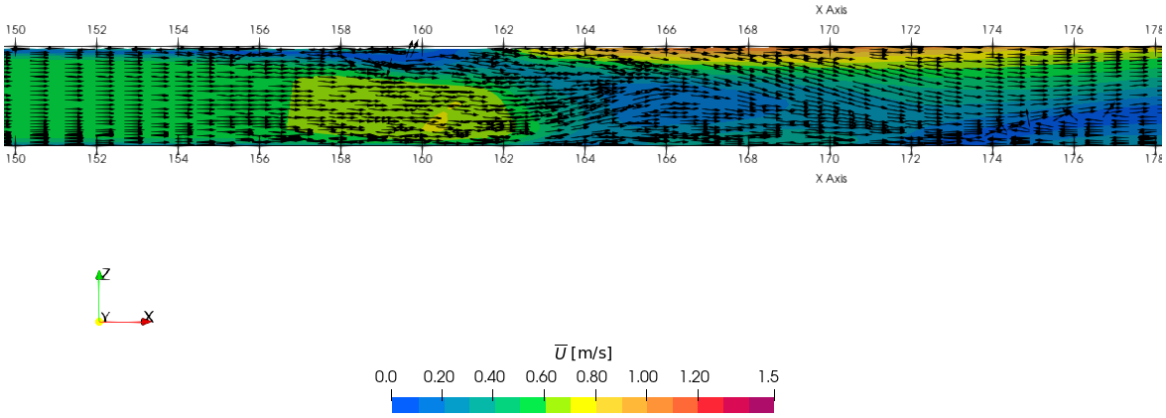

Figure 36 – Vertical Plane at Section 8.

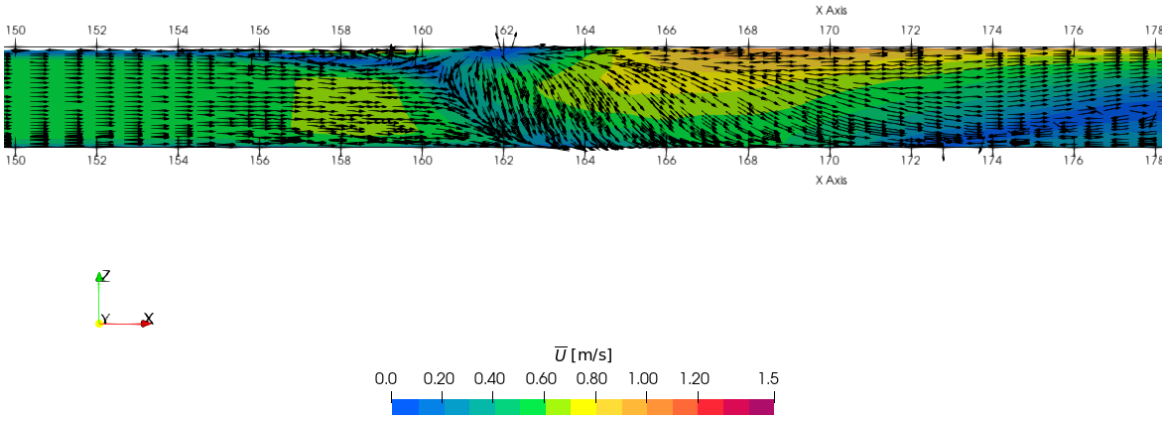

Figure 37 – Vertical Plane at Section 9.

A2.1.2 ALTERNATIVE 1 Case

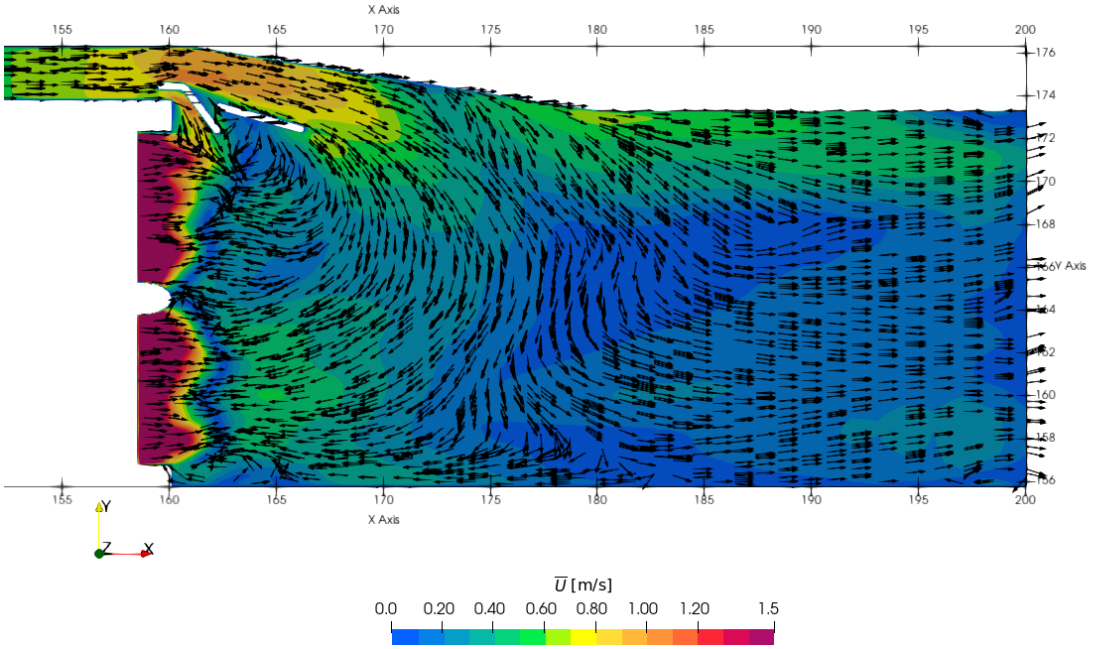

Figure 38 – Horizontal plane at Z = 5.5 mTAW.

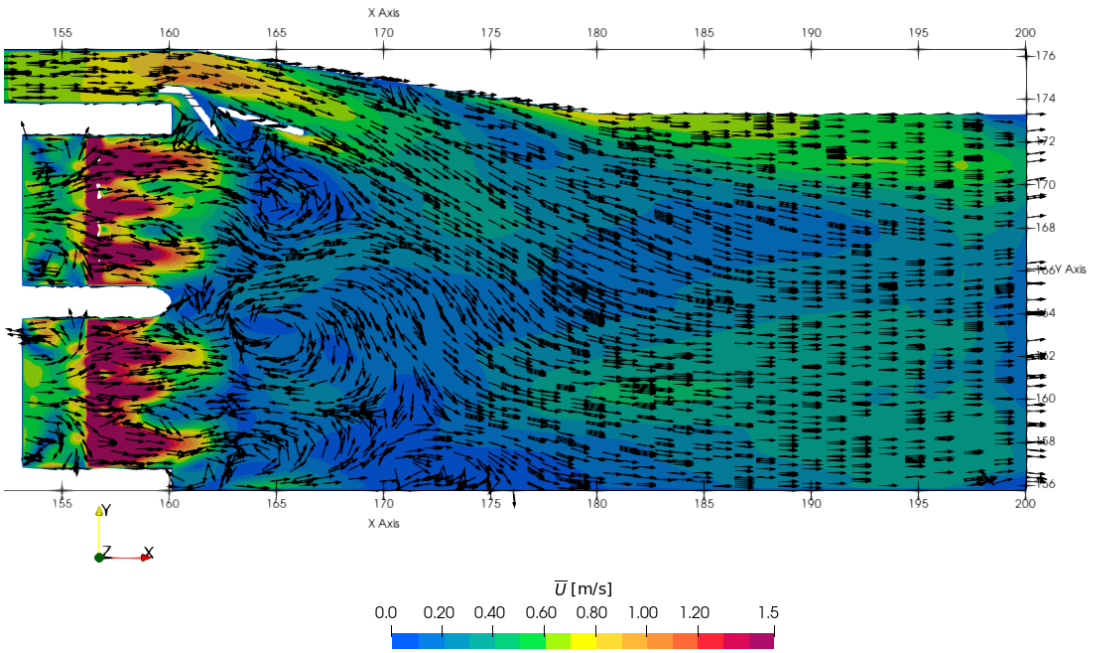

Figure 39 – Horizontal plane at Z = 6.0 mTAW.

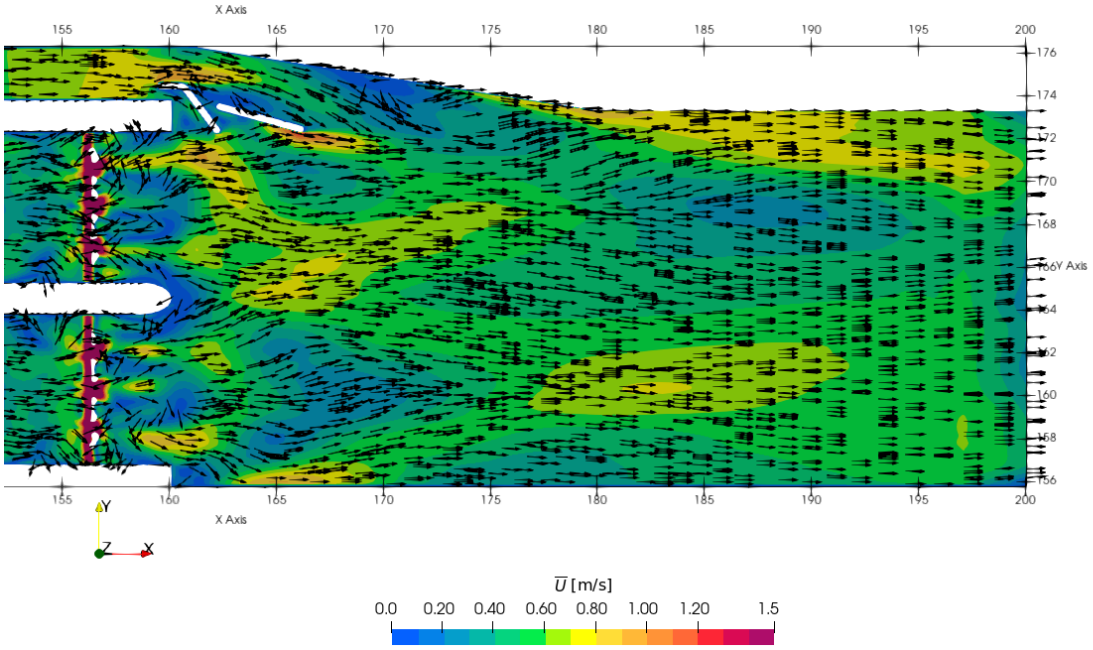

Figure 40 – Horizontal plane at Z = 6.5 mTAW.

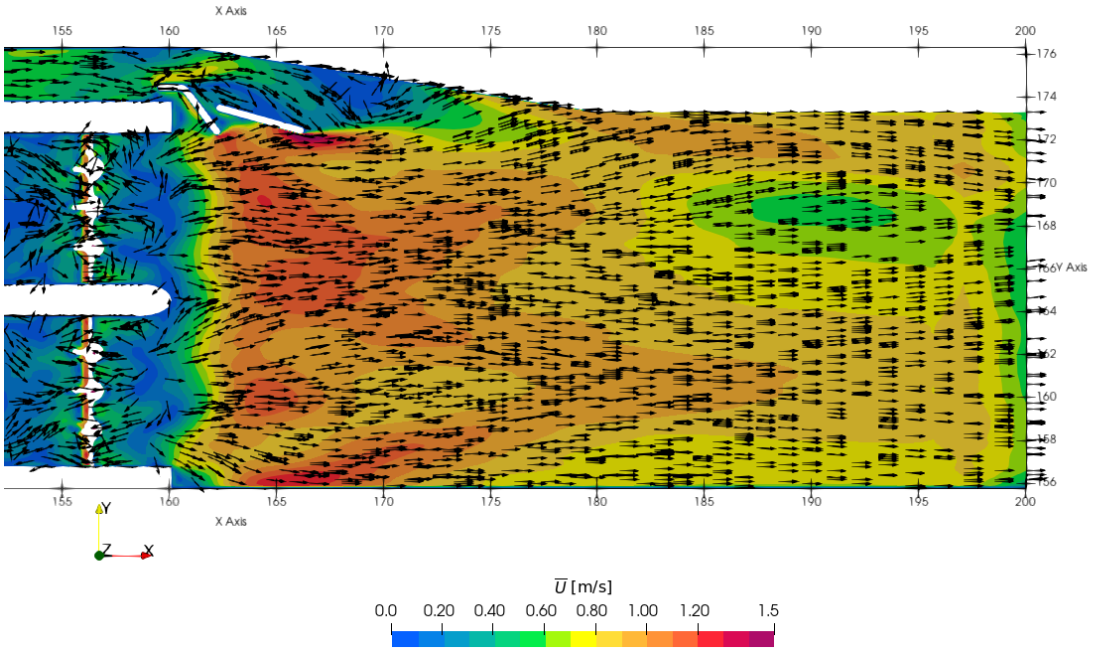

Figure 41 – Horizontal plane at Z = 7.0 mTAW.

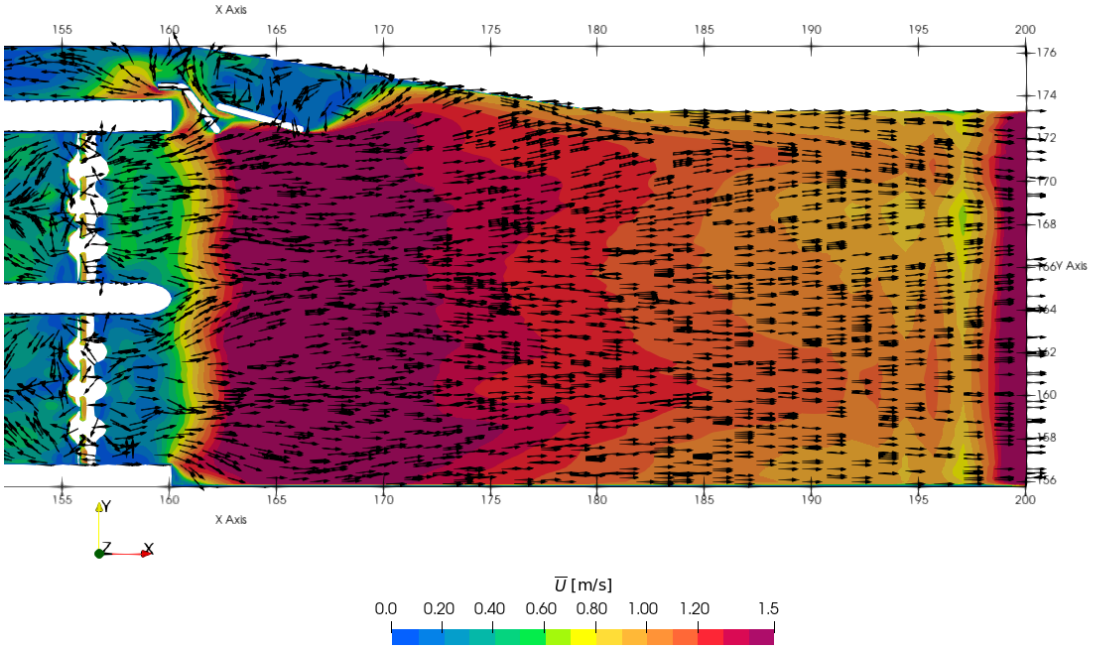

Figure 42 – Horizontal plane at Z = 7.5 mTAW.

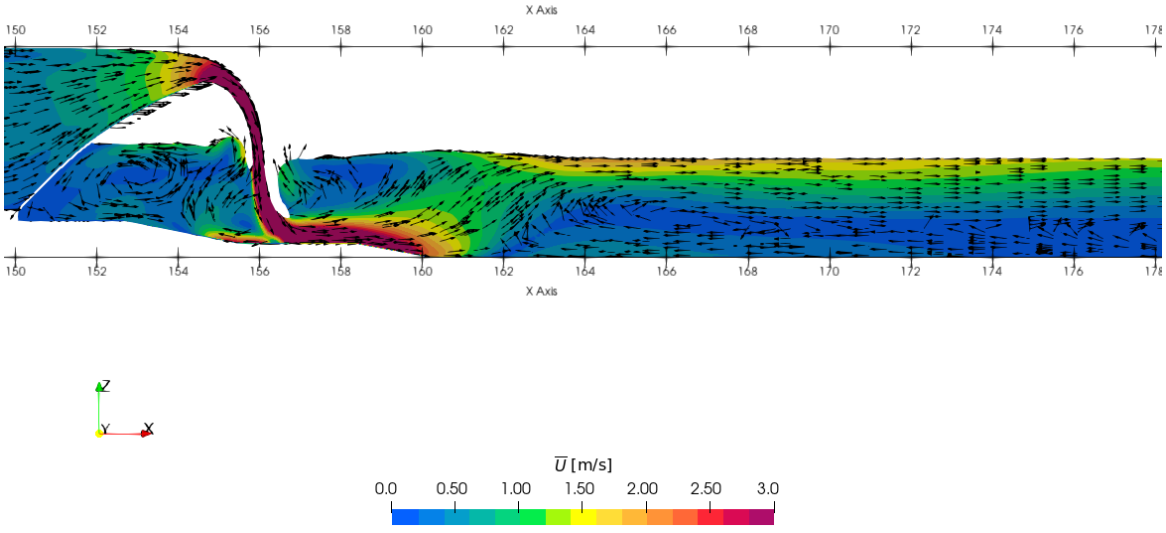

Figure 43 – Vertical Plane at Section 1.

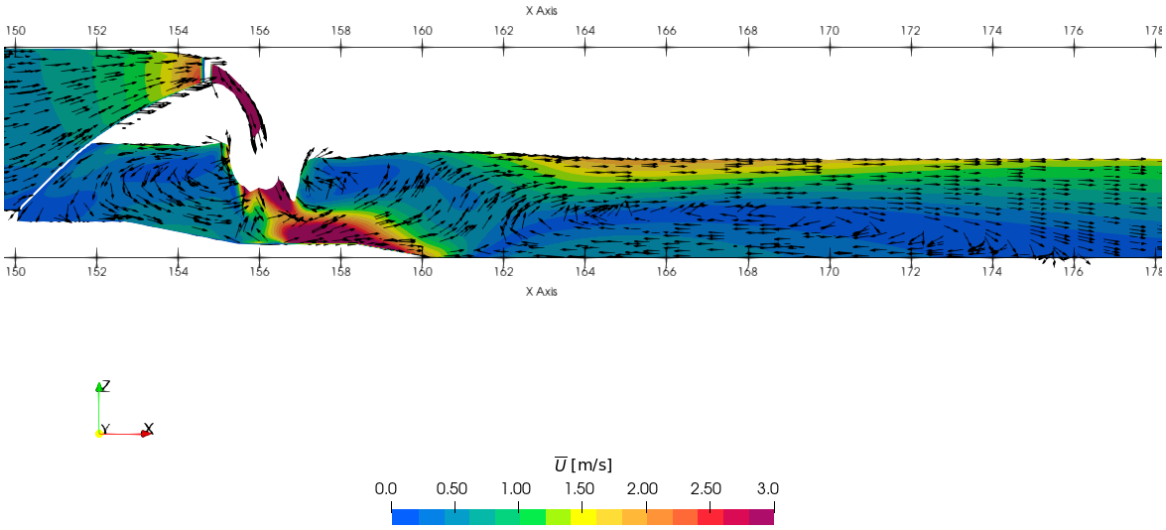

Figure 44 – Vertical Plane at Section 2.

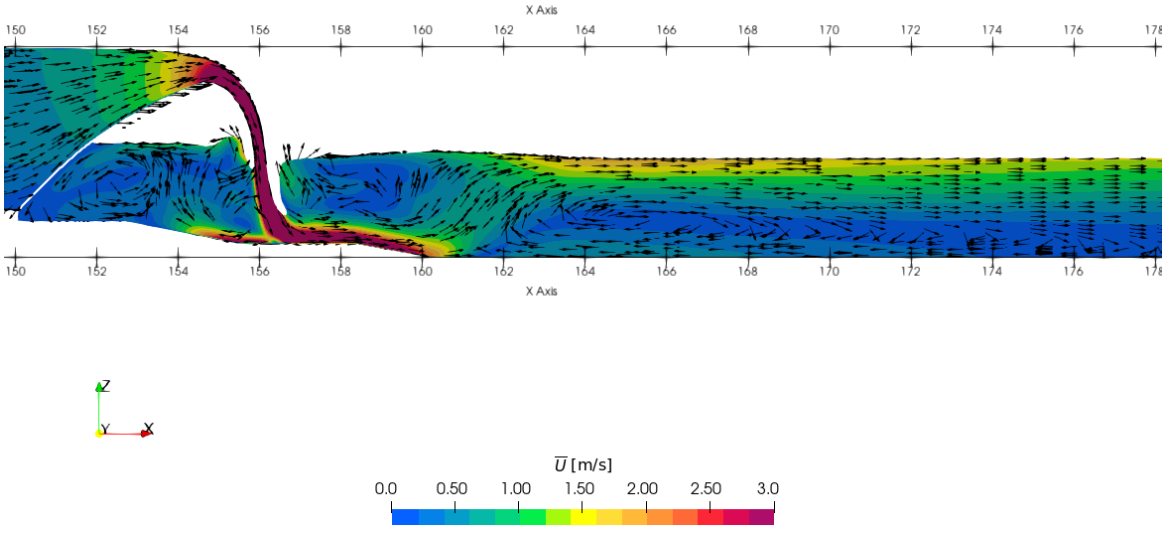

Figure 45 – Vertical Plane at Section 3.

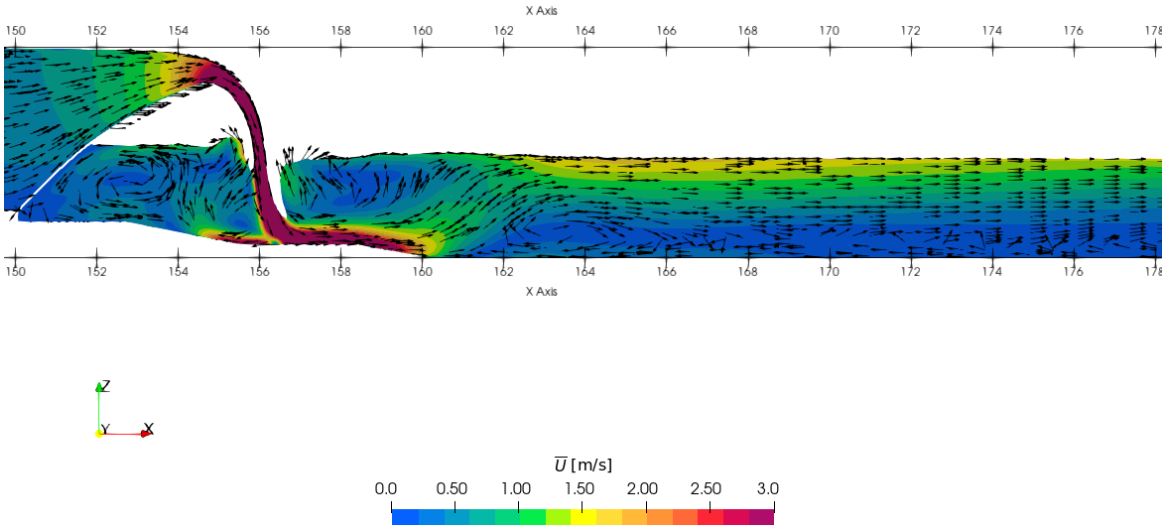

Figure 46 – Vertical Plane at Section 4.

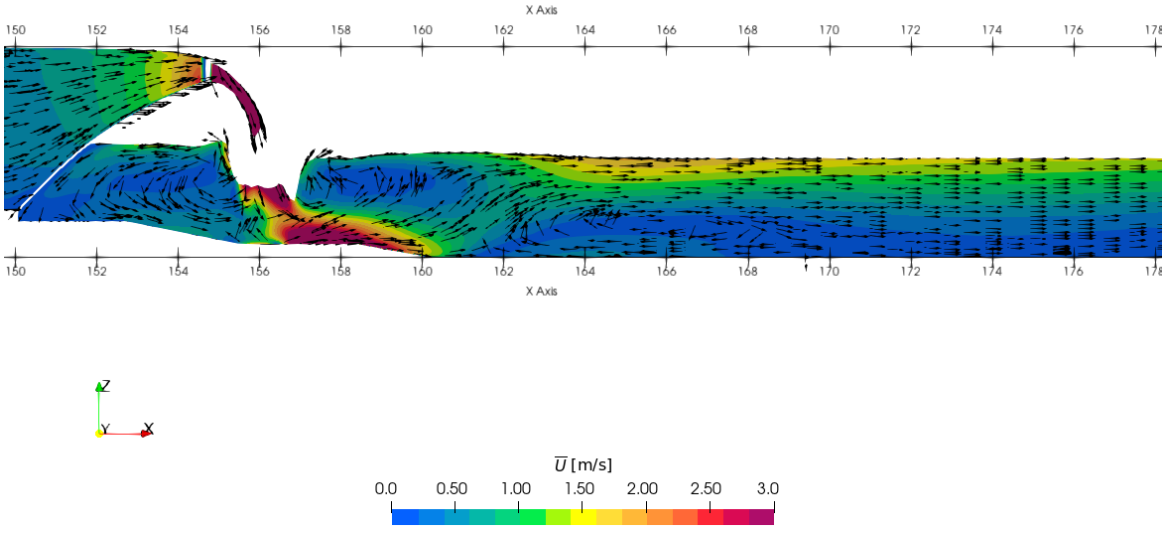

Figure 47 – Vertical Plane at Section 5.

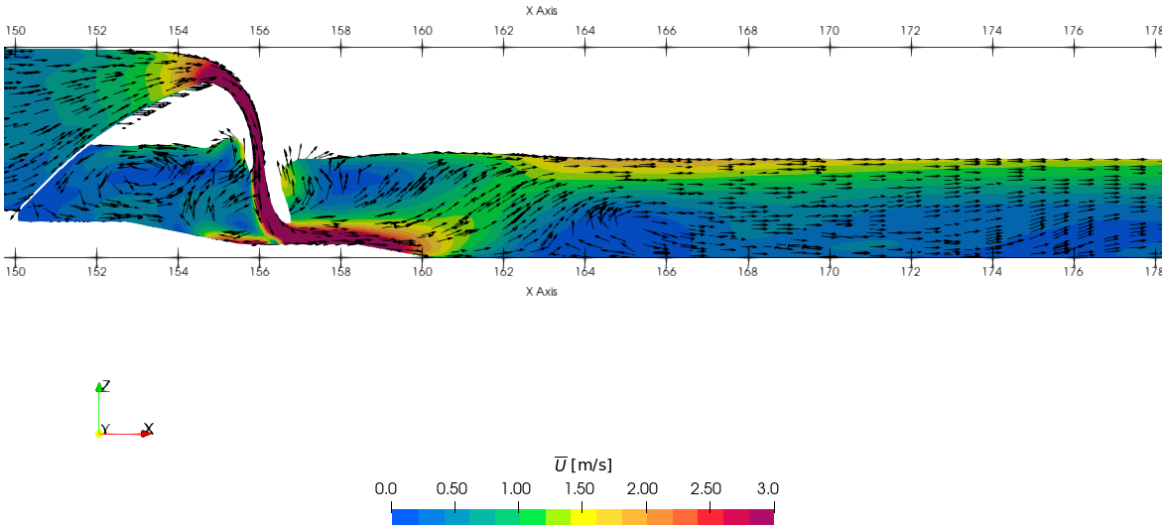

Figure 48 – Vertical Plane at Section 6.

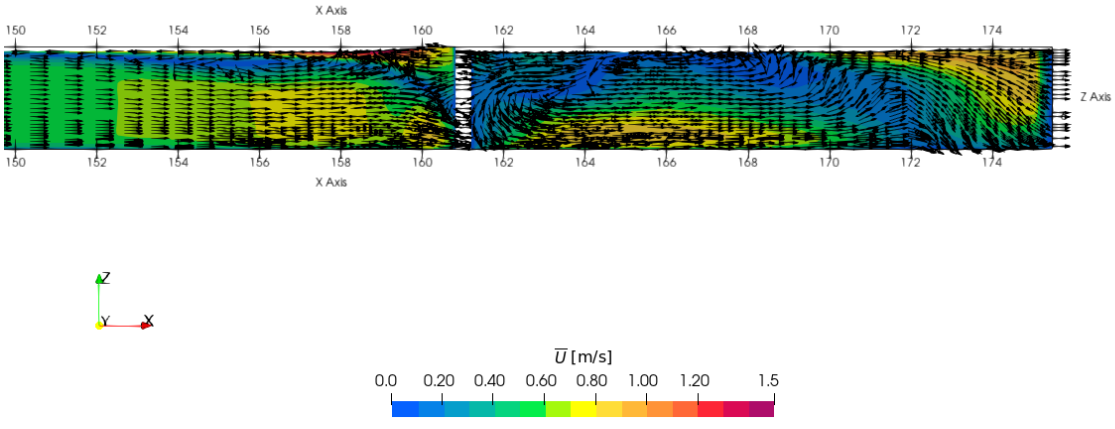

Figure 49 – Vertical Plane at Section 7.

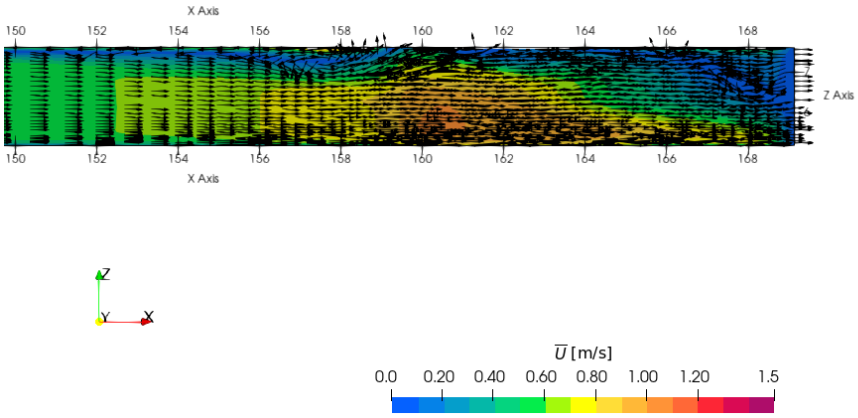

Figure 50 – Vertical Plane at Section 8.

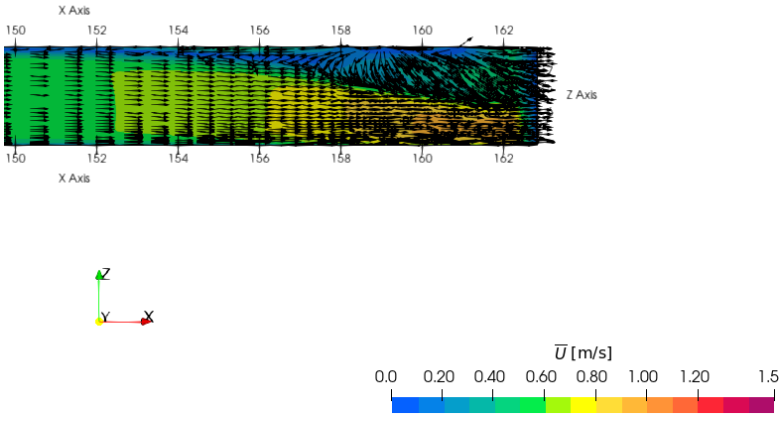

Figure 51 – Vertical Plane at Section 9.

DEPARTMENT **MOBILITY & PUBLIC WORKS**
Flanders Hydraulics

Berchemlei 115, 2140 Antwerp
T +32 (0)3 224 60 35
F +32 (0)3 224 60 36
waterbouwkundiglabo@vlaanderen.be
www.flandershydraulics.be